REPORT

Bi-allelic *CCDC47* Variants Cause a Disorder Characterized by Woolly Hair, Liver Dysfunction, Dysmorphic Features, and Global Developmental Delay

Marie Morimoto,[1,15] Helen Waller-Evans,[2,15] Zineb Ammous,[3,15] Xiaofei Song,[4,15] Kevin A. Strauss,[5] Davut Pehlivan,[4] Claudia Gonzaga-Jauregui,[6] Erik G. Puffenberger,[5] Charles R. Holst,[7] Ender Karaca,[4] Karlla W. Brigatti,[5] Emily Maguire,[2] Zeynep H. Coban-Akdemir,[4] Akiko Amagata,[7] C. Christopher Lau,[1] Xenia Chepa-Lotrea,[1] Ellen Macnamara,[1] Tulay Tos,[8] Sedat Isikay,[9] Michele Nehrebecky,[1] John D. Overton,[6] Matthew Klein,[7] Thomas C. Markello,[1] Jennifer E. Posey,[4] David R. Adams,[1,10,11] Emyr Lloyd-Evans,[2] James R. Lupski,[4,12,13,14] William A. Gahl,[1,10,11] and May Christine V. Malicdan[1,10,11,*]

Ca^{2+} signaling is vital for various cellular processes including synaptic vesicle exocytosis, muscle contraction, regulation of secretion, gene transcription, and cellular proliferation. The endoplasmic reticulum (ER) is the largest intracellular Ca^{2+} store, and dysregulation of ER Ca^{2+} signaling and homeostasis contributes to the pathogenesis of various complex disorders and Mendelian disease traits. We describe four unrelated individuals with a complex multisystem disorder characterized by woolly hair, liver dysfunction, pruritus, dysmorphic features, hypotonia, and global developmental delay. Through whole-exome sequencing and family-based genomics, we identified bi-allelic variants in *CCDC47* that encodes the Ca^{2+}-binding ER transmembrane protein CCDC47. CCDC47, also known as calumin, has been shown to bind Ca^{2+} with low affinity and high capacity. In mice, loss of *Ccdc47* leads to embryonic lethality, suggesting that Ccdc47 is essential for early development. Characterization of cells from individuals with predicted likely damaging alleles showed decreased *CCDC47* mRNA expression and protein levels. *In vitro* cellular experiments showed decreased total ER Ca^{2+} storage, impaired Ca^{2+} signaling mediated by the IP_3R Ca^{2+} release channel, and reduced ER Ca^{2+} refilling via store-operated Ca^{2+} entry. These results, together with the previously described role of CCDC47 in Ca^{2+} signaling and development, suggest that bi-allelic loss-of-function variants in *CCDC47* underlie the pathogenesis of this multisystem disorder.

Ca^{2+} signaling is a multipurpose intracellular signaling system that regulates a number of cellular processes including synaptic vesicle exocytosis, muscle contraction, regulation of secretion, transcription, and cellular proliferation.[1] The endoplasmic reticulum (ER), or the sarcoplasmic reticulum (SR) in muscle cells, is the largest store of intracellular Ca^{2+}.[2] ER Ca^{2+} depletion is also observed in a number of genetic disorders due to variants in Ca^{2+} channels and sensors. For example, Brody myopathy (MIM: 601003) is caused by recessive variants in *ATP2A1* (MIM: 611974), which encodes the fast-twitch skeletal muscle sarcoplasmic reticulum Ca^{2+} ATPase (SERCA1),[3] while Darier disease (MIM: 124200) occurs due to variants in *ATP2A2* (MIM: 108740), which encodes another sarcoplasmic reticulum Ca^{2+} ATPase, SERCA2.[4] Minicore myopathy (MIM: 255320) and central core disease (MIM: 117000) result from variants in *RYR1* (MIM: 180901), which encodes a major Ca^{2+} release channel,[5] and autosomal centronuclear myopathy (MIM: 160150) is associated with variants in *MTMR14* (MIM: 611089), which encodes a muscle-specific inositol phosphatase.[6] Stormorken syndrome (MIM: 185070), tubular aggregate myopathy 1 (MIM: 160565), and immunodeficiency 10 (MIM: 612783) are caused by variants in *STIM1* (MIM: 605921),[7–9] which encodes a Ca^{2+} sensor. Tubular aggregate myopathy 2 (MIM: 615883) and immunodeficiency 9 (MIM: 612782) are caused by variants in *ORAI1* (MIM: 610277),[10,11] which encodes a Ca^{2+} channel that coordinates ER Ca^{2+} refilling via store-operated Ca^{2+} entry (SOCE). Additionally, disruption of ER Ca^{2+} homeostasis contributes to the pathogenesis of several common diseases including diabetes mellitus, neurological diseases, and cancer.[12]

CCDC47, also known as calumin, is present in several tissues including brain, lung, heart, stomach, liver, spleen, kidney, muscle, and testis.[13] CCDC47 is an ER transmembrane Ca^{2+}-binding protein involved in embryogenesis and development.[13,14] A reported *Ccdc47*-knockout mouse model exhibited delayed development, atrophic neural

[1]National Institutes of Health Undiagnosed Diseases Program, Common Fund, Office of the Director, National Institutes of Health, Bethesda, MD 20892, USA; [2]School of Biosciences, Cardiff University, Cardiff CF10 3AX, UK; [3]The Community Health Clinic, Topeka, IN 46571, USA; [4]Department of Molecular and Human Genetics, Baylor College of Medicine, Houston, TX 77030, USA; [5]Clinic for Special Children, Strasburg, PA 17579, USA; [6]Regeneron Genetics Center, Regeneron Pharmaceuticals Inc., Tarrytown, NY 10591, USA; [7]BioElectron Technology Corporation, Mountain View, CA 94043, USA; [8]Department of Medical Genetics, Dr. Sami Ulus Research and Training Hospital of Women's and Children's Health and Diseases, Ankara 06080, Turkey; [9]Department of Physiotherapy and Rehabilitation, Hasan Kalyoncu University, School of Health Sciences, Gaziantep 27000, Turkey; [10]Medical Genetics Branch, National Human Genome Research Institute, National Institutes of Health, Bethesda, MD 20892, USA; [11]Office of the Clinical Director, National Human Genome Research Institute, National Institutes of Health, Bethesda, MD 20892, USA; [12]Department of Pediatrics, Baylor College of Medicine, Houston, TX 77030, USA; [13]Human Genome Sequencing Center, Baylor College of Medicine, Houston, TX 77030, USA; [14]Texas Children's Hospital, Houston, TX 77030, USA
[15]These authors contributed equally to this work
*Correspondence: maychristine.malicdan@nih.gov
https://doi.org/10.1016/j.ajhg.2018.09.014.

Table 1. Summary of Clinical Features of Individuals with Bi-allelic Loss-of-Function *CCDC47* Variants

Clinical Features	Proband 1	Proband 2	Proband 3	Proband 4
Prenatal and Perinatal History				
Delivery	C-section	C-section	NSVD	C-section
Premature birth	+	term	term	term
Polyhydramnios	+	–	–	–
Respiratory distress	–	NA	+	+
Decreased fetal movements	NA	+	+	NA
Bradycardia	+	+	–	+
Birth weight (%ile)	75th	NA	<3rd	10th
Growth Parameters				
Decreased body weight	+	+	+	+
Microcephaly	+	+	+	+
Physical Findings				
Coarse facies	+	+	+	+
Midface hypoplasia	+	+	+	–
Hypertelorism	+	+	+	–
Almond-shaped palpebral fissure	+	+	–	–
Epicanthal folds	–	–	+	–
Ptosis	+	+	+	+
Long eyelashes	+	+	–	–
Synophrys	+	–	+	+
Ectropion	+	+	–	–
Unusual nose	+	+	+	+
Downturned mouth	+	+	+	+
Macrostomia	–	+	wide mouth	–
Macroglossia	–	+	+	+
Full or thick lips	+	+	+	+
Dental abnormalities	+	–	+	+
High arched palate	+	+	+	+
Ear abnormalities	+	+	+	+
Bilateral otitis media	+	+	+	+
Bitemporal narrowing	–	+	+	+
Brachycephaly	+	+	+	+
Plagiocephaly	+	+	+	–
Pruritus	+	+	+	+
Unusual hair	+	+	+	+
Thoracic hypertrichosis	+	+	+	+
Fifth digit hypoplasia and/or clinodactyly	+	+	+	+
Dystrophic nails	–	–	+	–
Overlapping toes	+	+	+	+
Distal arthrogryposis / joint laxity	+	+	+	+
Hypoplastic nipples	+	+	+	+

(*Continued on next page*)

Table 1. ***Continued***

Clinical Features	Proband 1	Proband 2	Proband 3	Proband 4
Genital anomaly	+	+	–	–
Musculoskeletal Findings				
Hypotonia	+	+	+	+
Bilateral hip dislocation	+	+	ND	–
Hip dysplasia	+	+	ND	+
Bilateral coxa valga	+	–	ND	+
Abnormal bone density	+	+	ND	ND
Narrow chest	+	+	–	–
Fibular bowing	+	+	–	–
Genu valgum	–	–	+	–
Bilateral clubfoot	+	+	–	+
Small feet	+	+	+	+
Pectus excavatum	+	–	–	+
Scoliosis	–	+	+	–
Ocular Findings				
Hyperopia	+	NA	–	+
Astigmatism	+	NA	–	–
Cortical visual impairment	+	NA	+	+
Immunological Findings				
Recurrent infections	–	+	+	–
Immunodeficiency	–	+	+	–
Endocrine Findings				
Hypothyroidism	–	NA	+	–
Rickets	–	+	+	–
Respiratory Findings				
Obstructive sleep apnea	+	+	+	–
Central sleep apnea	+	NA	+	–
Heart Findings				
Ventricular septal defect	–	+	–	–
Patent ductus arteriosus	+	+	–	–
Gastrointestinal Findings				
Hepatosplenomegaly	+	–	+	–
Liver dysfunction	+	ND	+	+
Recurrent pancreatitis	+	NA	–	–
Exocrine pancreatic insufficiency	+	NA	–	–
Gastresophageal reflux	+	NA	+	+
Steatorrhea	+	+	–	–
Chronic diarrhea	–	+	–	+
Gallstones	+	–	–	+
Gastrostomy tube	+	–	+	+

(*Continued on next page*)

Table 1. ***Continued***

Clinical Features	Proband 1	Proband 2	Proband 3	Proband 4
Elevated bile acids	+	NA	+	+
Renal Findings				
Renal abnormalities	+	+	–	–
Neurological Findings				
Severe global developmental delay	+	+	+	+
Hyperreflexia	–	–	+	+
Reduced tendon reflexes	+	+	–	–
Absent Achilles reflex	+	+	–	–
Behavioral issues	–	–	+	+
Seizures	–	NA	+	–
EEG abnormalities	+	NA	+	+
Neuroimaging Findings				
Abnormal ventricle morphology	+	+	–	+
Abnormal corpus callosum	+	–	–	+
Cerebral atrophy	+	+	+	+
White matter abnormalities	–	–	–	+
Cerebellar hypoplasia	–	–	–	+

Abbreviations: +, present; – absent; C-section, Caesarean section; EEG, electroencephalogram; NA, not available; ND, not done; NSVD, normal spontaneous vaginal delivery.

tubes, heart abnormalities, a paucity of blood cells in the dorsal aorta, and embryonic lethality.[14] Further, mouse embryonic fibroblasts (MEFs) from these mice exhibited impaired Ca^{2+} signaling.[13] These data suggest that CCDC47 is critical for Ca^{2+} signaling and normal development.

In this study, we report four unrelated individuals presenting with a complex multisystem disorder characterized by woolly hair, liver dysfunction, pruritus, dysmorphic features, hypotonia, and global developmental delay; the clinical features of the probands are summarized in Table 1. We performed molecular analyses on probands who were referred to one of the collaborating centers for diagnostic evaluation of an undiagnosed genetic disorder and for whom prior genetic testing had been unrevealing. The parents of probands 1, 3, and 4 provided informed consent for sample collection and molecular analyses under protocol 76-HG-0238 approved by the NHGRI Institutional Review Board. The family of proband 2 gave consent for research studies through the Baylor-Hopkins Center for Mendelian Genomics (BHCMG) initiative under protocol #H-29697 approved by the Institutional Review Board at Baylor College of Medicine. The families of probands 3 and 4 were recruited for research studies through the Clinic for Special Children under a Lancaster General Hospital Institutional Review Board-approved protocol. Blood samples were collected from the probands and their unaffected parents and, when available, their unaffected siblings for whole-exome sequencing. Skin biopsies or peripheral blood leukocytes were obtained from the proband when possible for further molecular analyses. Using whole-exome sequencing, we identified bi-allelic variants in *CCDC47* that encodes the Ca^{2+}-binding ER transmembrane protein CCDC47. Further details on the methodologies used in this study are available in the Supplemental Data.

Proband 1 (1: II-1) was a 5-year-old female at the time she was evaluated through the National Institutes of Health Undiagnosed Diseases Program.[15–17] She was born to non-consanguineous parents of mixed Northern European and Native American descent. There were three miscarriages subsequent to the birth of proband 1. The pregnancy was complicated by premature rupture of membranes at 30 weeks of gestation, requiring preterm delivery by Caesarean section. At birth, she exhibited microcephaly, hypotonia, bilateral club foot deformities, and a patent ductus arteriosus (PDA). Complete blood counts identified anemia during infancy, which resolved by 5 years of age. She was unable to breast or bottle feed and was admitted to the NICU, where she was diagnosed with oral motor dyspraxia and severe gastresophageal reflux (GERD). At approximately 3 years of age, she experienced an episode of pancreatitis with liver inflammation. She had recurrent steatorrhea and low fecal elastase levels, and multiple gray-black cholesterol stones; cholecystectomy failed to resolve the problem and she underwent recurrent hospitalizations for similar episodes of pancreatitis. Evaluations for primary biliary cholangitis and autoimmune hepatitis were negative, and she was diagnosed with exocrine pancreatic

insufficiency. She had dysmorphic facial features including coarse and woolly hair, midface hypoplasia, hypertelorism, ptosis, a downturned mouth, full lips, dental abnormalities, a high arched palate, low-set ears, brachycephaly, and plagiocephaly (Figure 1A and Table 1). Further clinical examination revealed distal arthrogryposis, fifth digit hypoplasia, a narrow chest, hypoplastic nipples, hip dysplasia, clitoral hyperplasia, fibular bowing, and overlapping toes (Figure 1A and Table 1). Ophthalmologic evaluation showed astigmatism, hyperopia, and cortical visual impairment. Skeletal survey was consistent with osteopenia. She exhibited both truncal and appendicular hypotonia with poor head control and severe global developmental delay. She had frog leg posturing when supine. She could not hold objects, bear weight, or sit up without support. A brain MRI showed abnormalities of the corpus callosum as well as mild prominence of the third ventricle (Figure S1A). Additional clinical data are available in the Supplemental Note.

Proband 2 (2: II-3) was a male first seen by the Department of Medical Genetics at Dr. Sami Ulus Research and Training Hospital of Women's and Children's Health and Diseases at age 2 years 7 months. He was born at term via Caesarean section with a birth weight of 3,000 g. The parents were first-degree cousins of Turkish origin and they had two healthy living children and reported four previous miscarriages as well as two miscarriages subsequent to the birth of proband 2. The parents first noticed decreased spontaneous movements and hypotonia at 2 months of life. The infant had no head control and no single words. He was below the 3rd percentile for all anthropometric measurements, with severe malnutrition. Dysmorphic features included woolly and thin blonde hair, macroglossia, macrostomia, and simple large ears (Figure 1B and Table 1). The proband also exhibited bilateral cryptorchidism. Ophthalmologic evaluation was unremarkable. Laboratory studies including chemistry, blood count, metabolic testing (urine organic acid, ammonia, plasma amino acid, lactate, and pyruvate), congenital disorders of glycosylation testing, karyotype, and subtelomeric FISH were negative or inconclusive. Echocardiogram showed a ventricular septal defect (VSD) and PDA; abdominal ultrasound revealed nephrocalcinosis. Skeletal survey was consistent with osteoporosis (Figure S1B). Brain CT showed mild dilation of the lateral ventricles and cerebral atrophy. The boy was last evaluated at age 8 and the mother had two more miscarriages in the interim. He was referred to Baylor-Hopkins Center for Mendelian Genomics (BHCMG) to identify the molecular etiology.

Proband 3 (3: II-8) was an Old Order Amish female first seen at The Community Health Clinic (Topeka, IN) at age 7 years 7 months. She was born at 38 weeks of gestation via normal spontaneous vaginal delivery at home with a birth weight of 2,070 g and considered to be small for gestational age. The mother noticed slower and less frequent movements compared to her previous pregnancies. Due to respiratory distress, the newborn was transported to Wright Memorial Hospital (Trenton, MO) where she was placed on oxygen for 12–24 hr. She was frequently ill and diagnosed with failure to thrive (FTT); at 3 months of age a gastrostomy tube (G-tube) was placed. Dysmorphic features included microcephaly, dark and curly hair, epicanthal folds, hypertelorism, a bulbous nasal tip, and a wide and downturned mouth (Figure 1C and Table 1). She also had small hands and feet, dystrophic nails, and abnormal chubby toes that overlapped (Figure 1C and Table 1). The proband had a history of feeding issues, FTT, GERD, and liver dysfunction with mild splenomegaly and a prominent left hepatic lobe; itching improved on cholestyramine. She had recurrent infections due to a Toll-like receptor signaling defect, which was treated with IVIG, as well as central hypothyroidism and vitamin D-deficient rickets. Proband 3 also had chronic respiratory insufficiency and a history of apnea and sleep disturbances. Developmentally, she was severely delayed, nonverbal, and had generalized hypotonia. She could not grasp objects or sit up but was able to roll onto her side. Behaviorally, she displayed bruxism and self-mutilation; treatment with Risperdal resolved these behaviors. A brain MRI revealed mild prominence of the CSF space (Figure S1A). The parents had five healthy living children, two miscarriages, and two males who passed away at 3.5 months (3: II-3) due to aspiration pneumonia and at 7 months of gestation (3: II-6) (Figure 2A). A maternal uncle passed away at 9 weeks of age due to kidney failure. All had dark curly hair similar to proband 3 (3: II-8). Additional clinical data are available in the Supplemental Note.

Proband 4 (4: II-1) was first seen at The Community Health Clinic (Topeka, IN) at age 6 years 6 months. At birth, she was transferred to the Memorial Hospital NICU (South Bend, IN) for 5 days due to episodes of oxygen desaturation and poor feeding. At 1 year 6 months, she had a G-tube placed due to FTT. Her dysmorphic features included microcephaly, red curly hair, synophrys, full lips, and a downturned mouth (Figure 1D and Table 1). A skeletal survey showed that she had bilateral talipes equinovarus, coxa valga, bilateral overlapping toes, pectus excavatum, and hypermobile joints (Figure 1D and Table 1). Ophthalmologic evaluation showed she had hyperopia and cortical visual impairment. Proband 4 had abnormal liver function tests, elevated serum bile acids, and pruritus; itching improved on cholestyramine. She also had cholelithiasis without secondary evidence of acute cholecystitis; partial visualization of the pancreas was unremarkable. Neurologically, she had severe global developmental delay, hyperreflexia, hypotonia, and poor head control; she was non-verbal, although she sometimes answered "yah." She displayed bruxism and self-mutilation and also clapped or hit herself when excited. A brain MRI showed minimal prominence of the cerebral sulci and ventricular enlargement, global white matter paucity, and a thin corpus callosum (Figure S1A). The parents had three healthy living children subsequent to the birth of

Figure 1. Clinical Physical Features of the Four Probands with Bi-allelic Loss-of-Function *CCDC47* Variants
All four probands have dysmorphic facial features characterized by coarse facies, ptosis, a downturned mouth, simple ears, and unusual hair that is coarse and/or woolly and/or curly. Microcephaly, brachycephaly, hypotonia, joint laxity/distal arthrogryposis, nipple hypoplasia, and overlapping toes were also present in all of the probands. Other dysmorphic features observed in most of the probands include midface hypoplasia, hypertelorism, dental abnormalities, plagiocephaly, a narrow chest, hip dysplasia, and bilateral clubfoot.

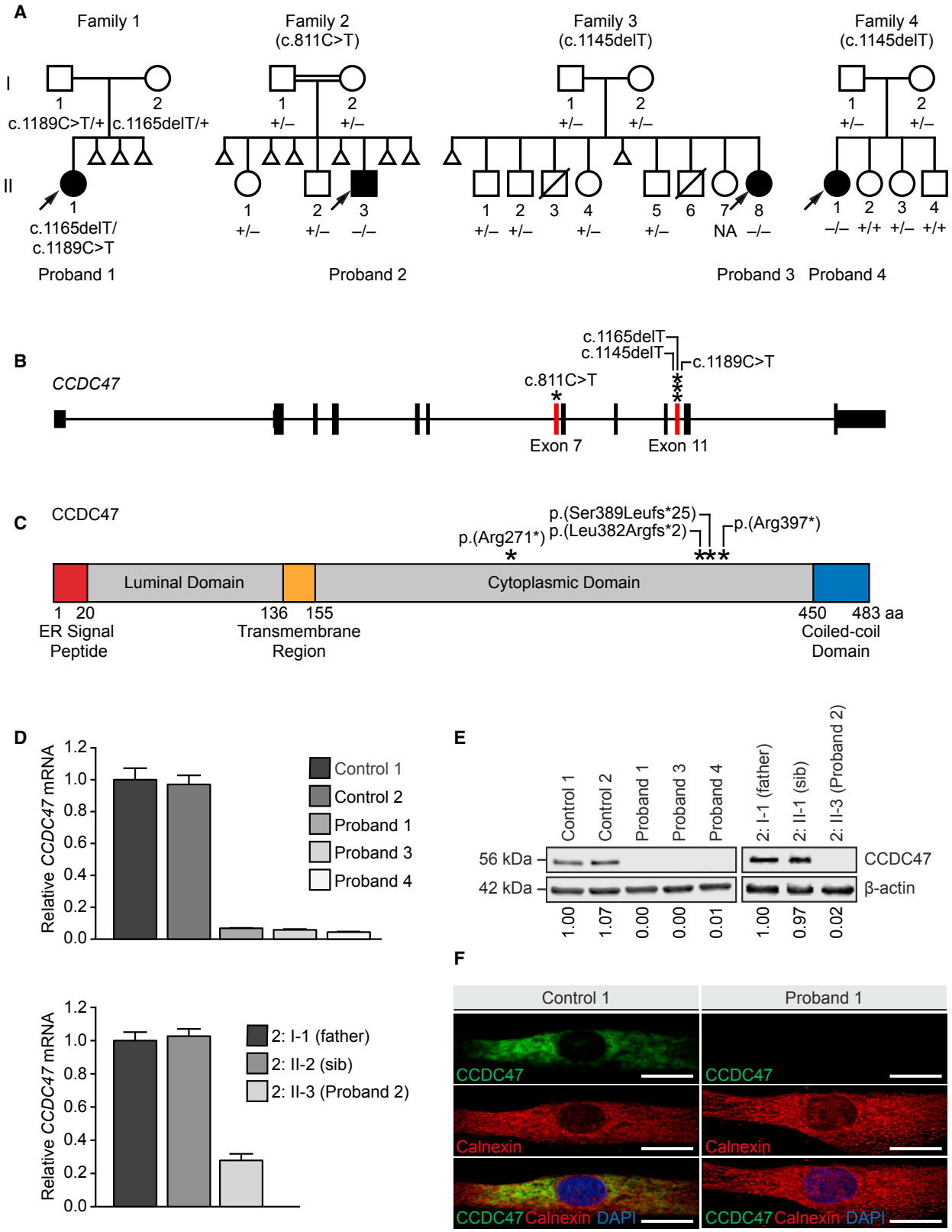

Figure 2. Bi-allelic *CCDC47* Variants Segregate with Disease in All Four Families and Lead to Decreased *CCDC47* mRNA Expression and CCDC47 Protein Levels

(A) The pedigrees of all four families with a proband exhibiting woolly hair, liver dysfunction, pruritus, dysmorphic features, and developmental delay show segregation of *CCDC47* (GenBank: NM_020198.2) variants in an autosomal-recessive mode of inheritance. Note recurrent pregnancy loss in three of four pedigrees.

(B) Schematic of *CCDC47* showing the locations of the variants (asterisks) leading to a frameshift or stop-gain variant in exon 7 and 11 (red bars).

(legend continued on next page)

the proband (Figure 2A). Additional clinical data are available in the Supplemental Note.

Whole-exome sequencing was performed on these four probands at three different research centers to identify pathogenic variants underlying their disease (Supplemental Subjects and Methods).[18] Variant interpretation and prioritization was based on the clinical relevance of the gene and the pathogenicity of the variants using ACMG-AMP guidelines.[19] Further variant prioritization was based on Mendelian consistency and segregation, observed frequency of the variants in public and internal population databases, conservation, and predicted deleteriousness coalesced with published biological and functional data of the candidate genes. Each center independently identified compound heterozygous or homozygous variants in *CCDC47* (GenBank: NM_020198.2) segregating according to Mendelian expectations for an autosomal-recessive disease trait (Figures 2A, 2B, and S2; Table 2). All of the *CCDC47* variants identified were either nonsense or frameshift variants that are predicted to lead to nonsense-mediated mRNA decay or premature truncation of the protein (Figure 2C and Table 2). The allele frequencies of the identified *CCDC47* variants in population databases, such as the Genome Aggregation Database (gnomAD), were very low ranging from 0.000% to 0.010% (Table 2) with no homozygotes recorded. In addition, these variants are predicted to be pathogenic by multiple bioinformatic algorithms (Table 2).

To experimentally assess the functional consequences of the variants identified, we performed TaqMan gene expression analysis to quantify *CCDC47* mRNA, western blot to assess the levels of CCDC47, and indirect immunofluorescence microscopy to assess the localization of the protein (Supplemental Subjects and Methods and Tables S1–S3). Gene expression analyses showed that the relative *CCDC47* mRNA was decreased in the primary dermal fibroblasts of probands 1 (1: II-1), 3 (3: II-8), and 4 (4: II-1) compared to two unaffected sex-matched pediatric controls (Figure 2D, upper panel) and in the lymphoblastoid cells of proband 2 (2: II-3) compared to his father (2: I-1) and unaffected sibling (2: II-2) (Figure 2D, lower panel). Consistent with the predicted loss-of-function effect of the identified variants, CCDC47 levels were nearly undetectable in the cells from all four probands, as assessed using an antibody that recognizes the C terminus of CCDC47 (Figure 2E). These results were consistent using an antibody that recognizes the N terminus of CCDC47 (data not shown). Cell studies showed that CCDC47 was localized in an ER-like pattern in unaffected control cells and that the signal for CCDC47 was undetectable by immunofluorescence using primary dermal fibroblasts from proband 1 (Figure 2F), consistent with the observation from western blot experiments. Altogether, our experiments support the hypothesis that the variants in *CCDC47* lead to nonsense-mediated decay of the prematurely truncated transcripts and result in the absence of protein and a functional loss of CCDC47.

To further explore the functional effects of loss of CCDC47, we performed *in vitro* experiments to interrogate ER Ca^{2+} storage, Ca^{2+} release, and store-operated Ca^{2+} entry (SOCE). CCDC47 has been previously shown to bind Ca^{2+},[13] so we hypothesized that the loss of CCDC47 expression would lead to impaired ER Ca^{2+} storage, signaling, and refilling. We performed live-cell imaging using the cell-permeable Ca^{2+} indicator Fura-2-acetoxymethyl ester (Fura-2AM) to monitor the elevation of cytoplasmic Ca^{2+} following the addition of either the sarco/endoplasmic reticulum Ca^{2+}-ATPase (SERCA) inhibitor thapsigargin at a high concentration to completely deplete ER Ca^{2+} levels and assess total ER Ca^{2+}. In addition, IP_3 was used to induce Ca^{2+} release via the inositol 1,4,5-trisphosphate receptor (IP_3R), ryanodine to induce Ca^{2+} release via the ryanodine receptor (RyR), thapsigargin at a low concentration to determine ER Ca^{2+} leak, and thapsigargin at a high concentration to deplete ER Ca^{2+} levels followed by $CaCl_2$ to assess refilling via SOCE (Supplemental Subjects and Methods). Complete inhibition of SERCA, which transports Ca^{2+} from the cytoplasm into the ER, was achieved by the addition of 2 μM thapsigargin, which leads to rapid depletion of ER Ca^{2+} stores and reflects total ER Ca^{2+} levels.[20] Our results show that total ER Ca^{2+} was decreased in the primary dermal fibroblasts of all three probands tested compared to unaffected control cells (Figure 3A). Ca^{2+} release via IP_3R was decreased in the primary dermal fibroblasts of all three probands tested (Figure 3B), while Ca^{2+} release via RyR was decreased only in proband 1 compared to that of unaffected control

(C) Schematic of CCDC47, also known as calumin, and its functional domains showing the locations of the predicted amino acid changes (asterisks).
(D) Relative *CCDC47* mRNA expression was quantified by TaqMan assay in the fibroblast cells of two unaffected control subjects and probands 1, 3, and 4 (upper panel) and in the lymphoblastoid cells of the father (2: I-1) and unaffected sibling (2: II-2) of proband 2 and proband 2 himself (2: II-3, lower panel). Data are presented as the mean of four technical replicates relative to control 1 (upper panel) or the father of proband 2 (2: I-1, lower panel). Expression of *HPRT1* and *POLR2A* were used as internal controls to normalize gene expression; error bars represent one standard deviation.
(E) CCDC47 levels were quantified by western blot using an antibody against the C terminus of CCDC47 in the fibroblasts of two unaffected control subjects and probands 1, 3, and 4 (left panel) and in the lymphoblastoid cells of the father (2: I-1) and unaffected sibling (2: II-2) of proband 2 and proband 2 himself (2: II-3, right panel). Samples were quantified relative to control 1 (left panel) or the father of proband 2 (2: I-1) (right panel). Expression of β-actin levels were used as a loading control to normalize CCDC47 levels.
(F) CCDC47 localization (green) was assessed by indirect immunofluorescence microscopy in the fibroblasts of an unaffected control and proband 1. An antibody against calnexin (red) was used as an ER marker; DAPI (blue) was used to stain the nucleus.
Scale bar = 20 microns. Abbreviations: aa, amino acid; DAPI, 4′,6-diamidino-2-phenylindole; ER, endoplasmic reticulum; NA, not available.

Table 2. Summary of Bi-allelic Loss-of-Function Variants Identified in *CCDC47* (GenBank: NM_020198.2)

Proband	Ancestry	Reported Consanguinity	Nucleotide Change (hg19 genomic coordinates)	Coding Sequence Change	Amino Acid Change	Inheritance	Parent of Origin	gnomAD All	CADD Phred Score	AOH Region Containing Candidate (Mb)	Genomewide AOH (Mb)
1	Northern European/Native American	no	Chr17:g.61829694G>A	c.1189C>T	p.Arg397*	compound heterozygous	P	0.010%	40	NA	NA
			Chr17:g.61829718del	c.1165delT	p.Ser389Leufs*25		M	0.000%	34	NA	NA
2	Turkish	yes	Chr17:g.61833855G>A	c.811C>T	p.Arg271*	homozygous	both	0.001%	39	1.3	268.4
3	Amish	no	Chr17:g.61829738del	c.1145delT	p.Leu382Argfs*2	homozygous	both	0.002%	35	19.6	81.2
4	Amish	no	Chr17:g.61829738del	c.1145delT	p.Leu382Argfs*2	homozygous	both	0.002%	35	15.7	65.1

Abbreviations: AOH, absence of heterozygosity; CADD, Combined Annotation Dependent Depletion; gnomAD, Genome Aggregation Database; M, maternal; NA, not applicable; P, paternal.

subjects (Figure 3C). Although proband 4 has generally lower Ca^{2+} released after addition of ryanodine, the difference from control subjects was not statistically significant. Partial inhibition of SERCA by the addition of 0.2 μM thapsigargin unmasks ER Ca^{2+} leak, a constitutive process mediated via ion channels such as presenilin 1 and bax inhibitor 1.[21,22] ER Ca^{2+} leak was decreased in probands 1 and 4 compared to that of unaffected control subjects (Figure 3D). SOCE was decreased in all three probands tested (Figure 3E), which may indicate inefficient refilling of the ER store via Ca^{2+} entry across the plasma membrane. Overexpression of *CCDC47* in the primary dermal fibroblasts of proband 1 rescued ER Ca^{2+} storage, signaling, and refilling via SOCE (Figures 3 and S3). Together, these Ca^{2+} imaging studies demonstrated that ER Ca^{2+} stores are decreased, ER Ca^{2+} signaling is impaired, and ER Ca^{2+} refilling via SOCE is reduced in the cells of individuals with *CCDC47* variants, suggesting that CCDC47 is important for the maintenance of Ca^{2+} homeostasis and signaling in the ER.

In addition to acting as the largest intracellular Ca^{2+} store, the ER is a dynamic organelle that is involved in protein synthesis, folding, quality control, and secretion. Accumulation of unfolded proteins leads to ER stress and the activation of several signal transduction pathways collectively known as the unfolded protein response (UPR). Three key UPR pathways, including the IRE1α, ATF6, and PERK pathways, have been identified (Figure S4A).[23–26] ER stress leads to IRE1α phosphorylation and subsequent splicing of *XBP1*, which is translated into a transcription factor that translocates into the nucleus (Figure S4A, left panel); and/or the cleavage of ATF6 into a transcription factor that translocates into the nucleus (Figure S4A, center panel); and/or the phosphorylation of PERK and eIF2α that lead to the activation of ATF4, a transcription factor that translocates into the nucleus (Figure S4A, right panel) to induce the transcription of UPR target genes.[23–26] Similar to the observations reported in *Ccdc47*-knockout mouse embryonic fibroblasts (MEFs),[13] primary dermal fibroblasts derived from proband 1 exhibited normal activation of each of the three arms of the UPR upon ER stress with the SERCA inhibitor thapsigargin (Figures S4B–S4D), suggesting that the UPR is functional in these cells.

Ca^{2+} release from the ER to the mitochondria is critical for Ca^{2+}-dependent mitochondrial membrane protein function, mitochondrial division, and apoptosis activation.[27] Further, there is extensive cross talk between Ca^{2+} and reactive oxygen species (ROS) signaling systems, and dysfunction in either system might detrimentally affect the other system.[28] Since Ca^{2+} storage is reduced and signaling is impaired in the ER of fibroblasts from individuals with *CCDC47* variants, we postulated that they may be more susceptible to oxidative stress. To test this, we performed an oxidative stress assay (Supplemental Subjects and Methods). Compared to unaffected control dermal fibroblasts, primary dermal fibroblasts from proband 1

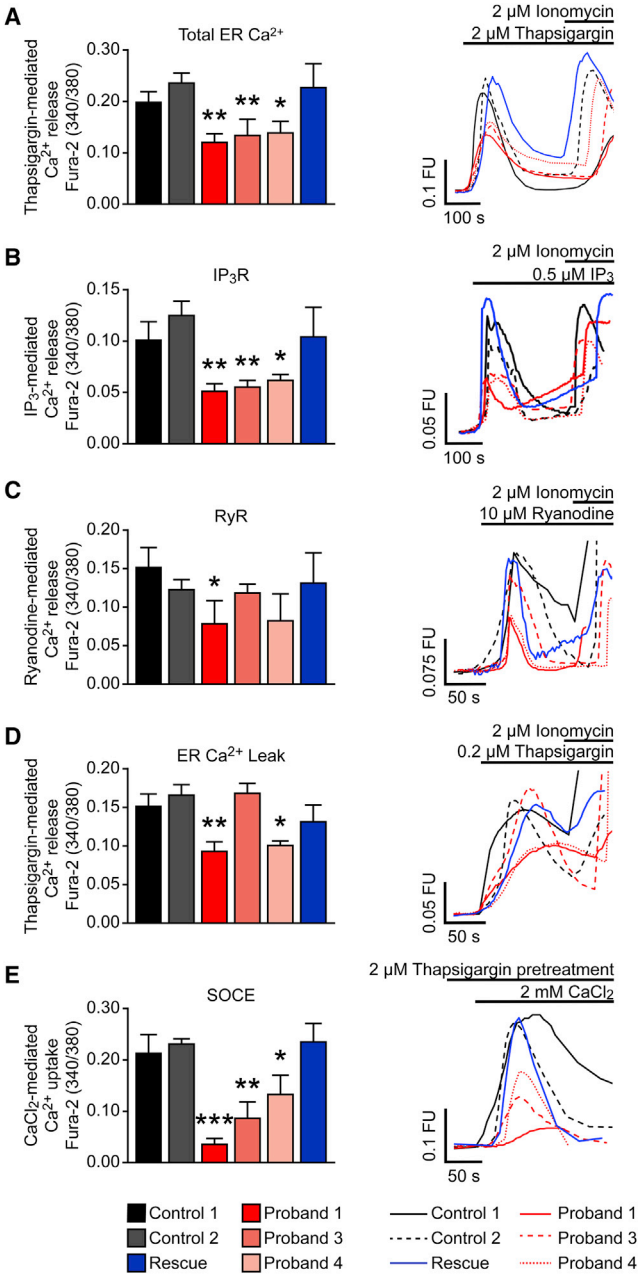

Figure 3. Total ER Ca^{2+} Storage, ER Ca^{2+} Signaling, and ER Ca^{2+} Refilling via Store-Operated Ca^{2+} Entry (SOCE) Are Impaired in Fibroblasts from Individuals with Loss-of-Function Variants in *CCDC47*

Unaffected control fibroblasts (control 1 and control 2), proband 1, 3, and 4 fibroblasts, and a rescue cell line where wild-type *CCDC47* was stably expressed in the dermal fibroblasts from proband 1 (Rescue) were stained and imaged live with the cytosolic Ca^{2+} probe Fura-2AM prior to the addition of 2 μM thapsigargin (A), 0.5 μM IP_3-AM (B), 10 μM ryanodine (C), 0.2 μM thapsigargin (D), or 2 mM $CaCl_2$ following 2 μM thapsigargin pretreatment (E) to measure the release of total Ca^{2+} from the ER, Ca^{2+} release from the ER via the inositol 1,4,5-triphosphate receptor (IP_3R), Ca^{2+} release from the ER via the ryanodine receptor (RyR), Ca^{2+} leak from the ER, or uptake of Ca^{2+} into the ER via SOCE, respectively. The selective Ca^{2+} ionophore ionomycin, which raises intracellular Ca^{2+} levels, was added to check cell viability. Representative graphs (left panels) and Ca^{2+} traces (right panels) summarizing Ca^{2+} release (A–D) or uptake (E) are shown. n = 3–7 with a minimum of 16 cells analyzed per experiment (A), n = 3–5 with a minimum of 8 cells analyzed per experiment (B), n = 3–8 with a minimum of 13 cells analyzed per experiment (C), n = 3–7 with a minimum of 14 cells analyzed per experiment (D), and n = 3–4 with a minimum of 16 cells analyzed per experiment (E). Error bars represent the standard error of the mean. *p < 0.05; **p < 0.01; ***p < 0.001. Abbreviations: FU, fluorescence units; s, seconds.

were more susceptible to oxidative stress in response to treatment with the glutathione synthesis inhibitor L-buthionine-(*S*,*R*)-sulfoximine (BSO) at a concentration of 50 μM and increasing concentrations of iron (Fe^{3+} citrate) to increase their oxidative burden (Figure S5A). Treatment with the antioxidant compound EPI-743, which has proven efficacy in rescuing cells from individuals with primary genetic mitochondrial disease,[29] rescued the phenotype of oxidative stress susceptibility with an EC_{50} of 19 nM in these primary dermal fibroblasts, while treatment with a non-redox cycling analog of EPI-743 (RS-743) showed no rescue from oxidative stress challenge when tested at concentrations up to 1,000 nM (Figure S5B). However, oxidative stress susceptibility was not increased in fibroblasts from probands 3 and 4, and proband 1 fibroblasts stably overexpressing wild-type *CCDC47* failed to rescue the molecular phenotype (data not shown). These findings suggest that CCDC47 deficiency does not uniformly lead to increased susceptibility to oxidative stress.

Through detailed clinical phenotyping, whole-exome sequencing analysis, and multicenter collaboration,[18] we identified four unrelated individuals with bi-allelic loss-of-function variants in *CCDC47* who are affected by a multisystem disorder characterized by woolly hair, liver dysfunction, pruritus, dysmorphic features, hypotonia, and global developmental delay (Figures 1, 2A, and 2B, and Table 1). The *CCDC47* variants identified in these four individuals are predicted to truncate CCDC47 (Figure 2C). Analyses of *CCDC47* mRNA and CCDC47 protein in cell lines derived from all four individuals demonstrated that both of these products were severely decreased or absent, supporting the prediction that these variants lead to nonsense-mediated decay and the consequent absence of the protein (Figures 2D–2F and Table 2). Further, we have demonstrated that Ca^{2+} storage, signaling, and refilling are impaired in primary dermal fibroblasts from individuals with bi-allelic loss-of-function variants in *CCDC47* (Figure 3), likely due to reduced levels of the ER Ca^{2+}-binding protein CCDC47. While additional candidate variants were detected in each of the probands (Table S4), *CCDC47* was the only candidate gene common to all four probands.

Of note, we observed some variability in the clinical presentation of the four probands reported in this study. First, proband 1 exhibited severe pancreatitis while the other individuals did not (Table 1). Her unique clinical presentation may be secondary to her gallbladder disease or her genetic background. Second, probands 2 and 3 presented with immunodeficiency and recurrent infections (Table 1). Given

that primary immunodeficiencies have been associated with variants in *STIM1* and *ORAI1* that encode key proteins involved in SOCE,[9,11] immunodeficiency may be a *bona fide* clinical feature of this disorder. Third, probands 3 and 4 exhibited several behavioral issues that the other two probands did not exhibit (Table 1); these behavioral issues might be due to a common change at another genetic locus, although no additional shared rare variants were identified through whole-exome sequencing of these probands. Fourth, proband 4 appears less severely affected compared to the three other probands. For instance, she was able to sit up and she did not have arthrogryposis or hypertelorism (Figure 1D and Table 1). Interestingly, proband 4 had the least severe SOCE molecular defect (Figure 3E). It is possible that there are genetic, environmental, and/or stochastic factors that lead to a variable clinical presentation among these four individuals. The identification and characterization of additional individuals will further help distill the key clinical features of this multisystem disorder that exhibits variable expressivity.

Notably, some of the rare *CCDC47* variants that we detected may be considered founder variants. Proband 2 is of Turkish ancestry with consanguineous parents and homozygous for a rare variant (c.811C>T [p.Arg271*]), whereas probands 3 and 4 are of Amish ancestry and, while unrelated, they both share homozygosis for the same rare variant (c.1145delT [p.Leu382Argfs*2]). These variants may be founder variants in the corresponding populations and, although maintained at very low frequencies, they are more likely to come together in homozygosis due to autozygosity by consanguinity, i.e., identity-by-descent or genetic drift in these populations. Indeed, the homozygous variant c.811C>T in proband 2 was located within a 1.3 Mb region of absence of heterozygosity (AOH) of a total of 268.4 Mb of autozygous genome, evidence of the reported consanguinity in this family (Table 2 and Figure S6A). AOH analyses of probands 3 and 4, both of Amish ancestry, revealed that the shared c.1145delT variant occurs within a 14.11 Mb shared haplotype within larger regions of AOH spanning 19.6 Mb and 15.7 Mb, respectively, in the genomes of these probands (Table 2 and Figure S6B). Therefore, these alleles can be readily included in population-specific disease panels for accurate and rapid molecular diagnosis and carrier or prenatal screening as reported for other founder alleles.[30]

The *Ccdc47*-knockout mouse model provides support for some of the clinical features we observed in our four unrelated individuals.[13,14] Similar to the *Ccdc47*-knockout mouse model, all of the individuals described in this study had decreased body weight and/or poor growth and neurological abnormalities including enlargement of the ventricles and/or cerebral atrophy; some of the individuals had heart abnormalities including PDA and/or VSD. Multiple miscarriages are a notable feature of all four families (Figure 2A). Interestingly, the *Ccdc47*-knockout mouse model generated on a mixed C57BL/6 × 129/Sv genetic background showed variable lethality ranging from embryonic to neonatal lethality.[13] Subsequent backcrossing of this line for more than six generations showed embryonic lethality at midgestation (E10.5–E11.5).[14] It is possible that some of the miscarried fetuses could also harbor bi-allelic variants in *CCDC47*. These observations suggest that there may be genetic modifiers of this clinical phenotype consistent with the variable expressivity observed in individuals with pathogenic *CCDC47* variants.

Ca^{2+} depletion of the ER can lead to ER stress and activation of the UPR pathways.[12] Despite Ca^{2+} depletion in the ER, we observed that the primary dermal fibroblasts derived from proband 1 were still capable of activating all three pathways of the UPR, including the IRE1α, ATF6, and PERK pathways, upon ER stress with thapsigargin similar to that of an unaffected control (Figure S4). Analogous findings have been observed in the *Ccdc47*-knockout MEFs.[13] Interestingly, activation of the IRE1α pathway and increased levels of the ER chaperone protein glucose-regulated protein 78 (GRP78), which is a key regulator of ER stress, an activator of UPR signaling, and a downstream target of UPR,[31,32] have been observed in *CCDC47*-knockdown HEK293 cells without treatment with thapsigargin.[14] These findings may be due in part to differences in cell type and/or due to an acute decrease in *CCDC47* levels.

Susceptibility to oxidative stress was increased in the primary dermal fibroblasts of proband 1, similar to what has been observed in individuals with primary mitochondrial disorders that affect cellular oxidation/reduction processes (Figure S5A). We postulated that the increased susceptibility to oxidative stress may be a secondary downstream effect of CCDC47 deficiency since Ca^{2+} signaling is integral for mitochondrial function and there is extensive crosstalk between the Ca^{2+} and ROS signaling systems.[27,28] However, we observed that fibroblasts from probands 3 and 4 did not show increased susceptibility to oxidative stress and fibroblasts from proband 1 stably overexpressing wild-type *CCDC47* were equally susceptible to oxidative stress as the fibroblasts from proband 1 lacking CCDC47. These findings strongly suggest that CCDC47 deficiency does not increase susceptibility to oxidative stress and that one or more variants, unique to proband 1, contribute to our observations.

Though most of the Ca^{2+} dysregulation disorders are myopathies, unsurprisingly due to the heavy Ca^{2+} dependency of muscle for contraction, we observed a broader and pleiotropic phenotype affecting multiple organs and systems beyond musculoskeletal findings in the case of CCDC47 deficiency. One explanation for the multisystem involvement is that a broader range of cell types and/or developmental stages, in addition to those involved in muscle contraction and development, may be sensitive to *CCDC47* deficiency. Since muscle contraction and synaptic vesicle exocytosis are regulated by Ca^{2+} signaling, it is possible that dysregulation of Ca^{2+} signaling due to CCDC47 deficiency could contribute to the hypotonia and global development delay in our probands. Gastrointestinal complications, including the cholestatic liver disease in probands 3 and 4, exocrine pancreatic insufficiency

in proband 1, and poor growth common to all four probands, are prominent clinical features (Table 1). Ca^{2+} signaling contributes to the regulation of secretion in many cell types, including hepatocytes and cholangiocytes that secrete bile, pancreatic acinar cells that secrete digestive enzymes, and salivary gland acinar cells that secrete saliva.[33–35] All three IP_3R isoforms are the primary Ca^{2+} release channels in the secretory cells of the bile duct, and the loss of IP_3R and subsequent loss of Ca^{2+} release has been shown to contribute to the pathogenesis of cholestatic liver disease.[36,37] Furthermore, mice in which type 2 and type 3 IP_3Rs are absent displayed secretion deficits in the pancreatic and salivary gland acinar cells due to impaired Ca^{2+} signaling that ultimately led to difficulties in nutrient digestion and poor growth.[38] Similarly, all of the individuals in this study presented with poor growth and most were fed by G-tube (Figure 1 and Table 1). Further studies performed in a clinically relevant cell type via *CCDC47*-knockdown cultured cells or in a conditional *Ccdc47*-knockout mouse model are required to delineate the molecular mechanism by which CCDC47 deficiency contributes to these clinical features.

Although we identified impaired Ca^{2+} homeostasis and signaling in primary dermal fibroblasts from individuals with bi-allelic loss-of-function variants in *CCDC47*, there are several other known proteins that have Ca^{2+} buffering capacity in the ER. Examples include calreticulin, heat shock protein 90 beta family member 1 (also known as endoplasmin or GRP94), calnexin, and prolyl 4-hydroxylase subunit beta (also known as protein disulfide isomerase).[39,40] Similar to CCDC47, these proteins bind Ca^{2+} with low affinity and high capacity.[13,41–47] In fact, calreticulin has been shown to bind approximately 50% of the total Ca^{2+} within the ER.[48] Many of these ER Ca^{2+} buffering proteins are multifunctional and, indeed, loss-of-function mouse models generated for several of these showed embryonic lethality,[49–51] which suggests that these proteins have non-overlapping functions. Therefore, it is probable that CCDC47 has yet unexplored and unique roles, aside from its ER Ca^{2+} buffering capacity, that cannot be compensated for by the presence of other Ca^{2+} buffering proteins in the ER. Indeed, CCDC47 has been suggested to regulate Ca^{2+} release-activated Ca^{2+} (CRAC) channels that are responsible for ER filling and interacts with STIM1 and ORAI1 that are responsible for SOCE.[52] Our molecular findings of decreased ER Ca^{2+} and SOCE align with those observed in the *Ccdc47*-knockout MEFs,[13] which suggests that CCDC47 may be involved in regulating SOCE.

In summary, we report that bi-allelic loss-of-function variants in *CCDC47* cause a rare autosomal-recessive disorder characterized by woolly hair, liver dysfunction, pruritus, dysmorphic features, and global developmental delay. Through *in vitro* and cellular experiments, we provide evidence that Ca^{2+} storage and signaling are impaired in primary dermal fibroblasts derived from three individuals with loss-of-function variants in *CCDC47*; however, it is not clear how CCDC47 deficiency leads to the clinical presentation observed in the affected individuals. Additional functional studies will be necessary to better understand the role of CCDC47 in Ca^{2+} homeostasis and signaling in the ER and further elucidate how its absence leads to this developmental disorder.

Accession Numbers

The accession numbers for the variants reported in this paper are ClinVar: SCV000809006, SCV000809007, SCV000809008, and SCV000809009.

Supplemental Data

Supplemental Data include Supplemental Note, Supplemental Subjects and Methods, six figures, and four tables and can be found with this article online at https://doi.org/10.1016/j.ajhg.2018.09.014.

Acknowledgments

We thank all of the individuals presented in the study and their families for their participation in this study. This study was supported in part by the National Human Genome Research Institute (NHGRI) Intramural Research Program; the National Institutes of Health (NIH) Common Fund from the Office of the Director; charitable contributions from Old Order Amish and Mennonite communities of Pennsylvania, Indiana, and surrounding states; the EU Horizon 2020 BATcure consortium grant (666918) to H.W.-E. and E.L.-E.; a research grant from The Royal Society to E.L.-E.; R35 NS105078 to J.R.L.; MDA#512848 to J.R.L.; and a jointly funded NHGRI and National Heart, Lung, and Blood Institute (NHLBI) grant to the Baylor-Hopkins Center for Mendelian Genomics (UM1 HG006542) to J.R.L. E.M. was supported by a PhD studentship from the Niemann-Pick Research Foundation; J.E.P. is supported by NHGRI K08 HG008986.

Declaration of Interests

C.R.H., A.A., and M.K. are employees of BioElectron Technology Corporation, which is developing EPI-743 for the treatment of mitochondrial disease and related disorders. C.G.-J. and J.D.O. are full-time employees of the Regeneron Genetics Center from Regeneron Pharmaceuticals Inc. and receive stock options as part of compensation. J.R.L. has stock ownership in 23andMe and Lasergen, is a paid consultant for Regeneron, and is a co-inventor on multiple United States and European patents related to molecular diagnostics for inherited neuropathies, eye diseases, and bacterial genomic fingerprinting. The other authors declare no conflicts of interest.

Received: June 19, 2018
Accepted: September 26, 2018
Published: October 25, 2018

Web Resources

CADD, https://cadd.gs.washington.edu/
ClinVar, https://www.ncbi.nlm.nih.gov/clinvar/
dbSNP, https://www.ncbi.nlm.nih.gov/projects/SNP/
ExAC Browser, http://exac.broadinstitute.org/

GenBank, https://www.ncbi.nlm.nih.gov/genbank/
gnomAD Browser, http://gnomad.broadinstitute.org/
Human Gene Mutation Database, http://www.hgmd.cf.ac.uk/ac/index.php
OMIM, http://www.omim.org/
PolyPhen-2, http://genetics.bwh.harvard.edu/pph2/
PubMed, http://www.ncbi.nlm.nih.gov/PubMed/
SIFT, http://sift.bii.a-star.edu.sg/

References

1. Berridge, M.J., Bootman, M.D., and Roderick, H.L. (2003). Calcium signalling: dynamics, homeostasis and remodelling. Nat. Rev. Mol. Cell Biol. *4*, 517–529.
2. Somlyo, A.P., Bond, M., and Somlyo, A.V. (1985). Calcium content of mitochondria and endoplasmic reticulum in liver frozen rapidly *in vivo*. Nature *314*, 622–625.
3. Odermatt, A., Taschner, P.E., Khanna, V.K., Busch, H.F., Karpati, G., Jablecki, C.K., Breuning, M.H., and MacLennan, D.H. (1996). Mutations in the gene-encoding SERCA1, the fast-twitch skeletal muscle sarcoplasmic reticulum Ca^{2+} ATPase, are associated with Brody disease. Nat. Genet. *14*, 191–194.
4. Sakuntabhai, A., Ruiz-Perez, V., Carter, S., Jacobsen, N., Burge, S., Monk, S., Smith, M., Munro, C.S., O'Donovan, M., Craddock, N., et al. (1999). Mutations in *ATP2A2*, encoding a Ca^{2+} pump, cause Darier disease. Nat. Genet. *21*, 271–277.
5. Zhang, Y., Chen, H.S., Khanna, V.K., De Leon, S., Phillips, M.S., Schappert, K., Britt, B.A., Browell, A.K., and MacLennan, D.H. (1993). A mutation in the human ryanodine receptor gene associated with central core disease. Nat. Genet. *5*, 46–50.
6. Shen, J., Yu, W.M., Brotto, M., Scherman, J.A., Guo, C., Stoddard, C., Nosek, T.M., Valdivia, H.H., and Qu, C.K. (2009). Deficiency of MIP/MTMR14 phosphatase induces a muscle disorder by disrupting $Ca(^{2+})$ homeostasis. Nat. Cell Biol. *11*, 769–776.
7. Misceo, D., Holmgren, A., Louch, W.E., Holme, P.A., Mizobuchi, M., Morales, R.J., De Paula, A.M., Stray-Pedersen, A., Lyle, R., Dalhus, B., et al. (2014). A dominant *STIM1* mutation causes Stormorken syndrome. Hum. Mutat. *35*, 556–564.
8. Böhm, J., Chevessier, F., Maues De Paula, A., Koch, C., Attarian, S., Feger, C., Hantaï, D., Laforêt, P., Ghorab, K., Vallat, J.M., et al. (2013). Constitutive activation of the calcium sensor STIM1 causes tubular-aggregate myopathy. Am. J. Hum. Genet. *92*, 271–278.
9. Picard, C., McCarl, C.A., Papolos, A., Khalil, S., Lüthy, K., Hivroz, C., LeDeist, F., Rieux-Laucat, F., Rechavi, G., Rao, A., et al. (2009). *STIM1* mutation associated with a syndrome of immunodeficiency and autoimmunity. N. Engl. J. Med. *360*, 1971–1980.
10. Endo, Y., Noguchi, S., Hara, Y., Hayashi, Y.K., Motomura, K., Miyatake, S., Murakami, N., Tanaka, S., Yamashita, S., Kizu, R., et al. (2015). Dominant mutations in ORAI1 cause tubular aggregate myopathy with hypocalcemia via constitutive activation of store-operated Ca^{2+} channels. Hum. Mol. Genet. *24*, 637–648.
11. Feske, S., Gwack, Y., Prakriya, M., Srikanth, S., Puppel, S.H., Tanasa, B., Hogan, P.G., Lewis, R.S., Daly, M., and Rao, A. (2006). A mutation in *Orai1* causes immune deficiency by abrogating CRAC channel function. Nature *441*, 179–185.
12. Mekahli, D., Bultynck, G., Parys, J.B., De Smedt, H., and Missiaen, L. (2011). Endoplasmic-reticulum calcium depletion and disease. Cold Spring Harb. Perspect. Biol. *3*, 3.
13. Zhang, M., Yamazaki, T., Yazawa, M., Treves, S., Nishi, M., Murai, M., Shibata, E., Zorzato, F., and Takeshima, H. (2007). Calumin, a novel Ca^{2+}-binding transmembrane protein on the endoplasmic reticulum. Cell Calcium *42*, 83–90.
14. Yamamoto, S., Yamazaki, T., Komazaki, S., Yamashita, T., Osaki, M., Matsubayashi, M., Kidoya, H., Takakura, N., Yamazaki, D., and Kakizawa, S. (2014). Contribution of calumin to embryogenesis through participation in the endoplasmic reticulum-associated degradation activity. Dev. Biol. *393*, 33–43.
15. Gahl, W.A., and Tifft, C.J. (2011). The NIH Undiagnosed Diseases Program: lessons learned. JAMA *305*, 1904–1905.
16. Gahl, W.A., Markello, T.C., Toro, C., Fajardo, K.F., Sincan, M., Gill, F., Carlson-Donohoe, H., Gropman, A., Pierson, T.M., Golas, G., et al. (2012). The National Institutes of Health Undiagnosed Diseases Program: insights into rare diseases. Genet. Med. *14*, 51–59.
17. Gahl, W.A., Mulvihill, J.J., Toro, C., Markello, T.C., Wise, A.L., Ramoni, R.B., Adams, D.R., Tifft, C.J.; and UDN (2016). The NIH Undiagnosed Diseases Program and Network: Applications to modern medicine. Mol. Genet. Metab. *117*, 393–400.
18. Sobreira, N., Schiettecatte, F., Valle, D., and Hamosh, A. (2015). GeneMatcher: a matching tool for connecting investigators with an interest in the same gene. Hum. Mutat. *36*, 928–930.
19. Richards, S., Aziz, N., Bale, S., Bick, D., Das, S., Gastier-Foster, J., Grody, W.W., Hegde, M., Lyon, E., Spector, E., et al.; ACMG Laboratory Quality Assurance Committee (2015). Standards and guidelines for the interpretation of sequence variants: a joint consensus recommendation of the American College of Medical Genetics and Genomics and the Association for Molecular Pathology. Genet. Med. *17*, 405–424.
20. Thastrup, O., Cullen, P.J., Drøbak, B.K., Hanley, M.R., and Dawson, A.P. (1990). Thapsigargin, a tumor promoter, discharges intracellular Ca^{2+} stores by specific inhibition of the endoplasmic reticulum $Ca^{2(+)}$-ATPase. Proc. Natl. Acad. Sci. USA *87*, 2466–2470.
21. Nelson, O., Tu, H., Lei, T., Bentahir, M., de Strooper, B., and Bezprozvanny, I. (2007). Familial Alzheimer disease-linked mutations specifically disrupt Ca^{2+} leak function of presenilin 1. J. Clin. Invest. *117*, 1230–1239.
22. Bultynck, G., Kiviluoto, S., and Methner, A. (2014). Bax inhibitor-1 is likely a pH-sensitive calcium leak channel, not a H^+/Ca^{2+} exchanger. Sci. Signal. *7*, pe22.
23. Harding, H.P., Zhang, Y., and Ron, D. (1999). Protein translation and folding are coupled by an endoplasmic-reticulum-resident kinase. Nature *397*, 271–274.
24. Haze, K., Yoshida, H., Yanagi, H., Yura, T., and Mori, K. (1999). Mammalian transcription factor ATF6 is synthesized as a transmembrane protein and activated by proteolysis in response to endoplasmic reticulum stress. Mol. Biol. Cell *10*, 3787–3799.
25. Yoshida, H., Matsui, T., Yamamoto, A., Okada, T., and Mori, K. (2001). *XBP1* mRNA is induced by ATF6 and spliced by IRE1 in response to ER stress to produce a highly active transcription factor. Cell *107*, 881–891.
26. Calfon, M., Zeng, H., Urano, F., Till, J.H., Hubbard, S.R., Harding, H.P., Clark, S.G., and Ron, D. (2002). IRE1 couples endoplasmic reticulum load to secretory capacity by processing the *XBP-1* mRNA. Nature *415*, 92–96.

27. Rowland, A.A., and Voeltz, G.K. (2012). Endoplasmic reticulum-mitochondria contacts: function of the junction. Nat. Rev. Mol. Cell Biol. *13*, 607–625.
28. Görlach, A., Bertram, K., Hudecova, S., and Krizanova, O. (2015). Calcium and ROS: A mutual interplay. Redox Biol. *6*, 260–271.
29. Shrader, W.D., Amagata, A., Barnes, A., Enns, G.M., Hinman, A., Jankowski, O., Kheifets, V., Komatsuzaki, R., Lee, E., Mollard, P., et al. (2011). α-Tocotrienol quinone modulates oxidative stress response and the biochemistry of aging. Bioorg. Med. Chem. Lett. *21*, 3693–3698.
30. Strauss, K.A., Gonzaga-Jauregui, C., Brigatti, K.W., Williams, K.B., King, A.K., Van Hout, C., Robinson, D.L., Young, M., Praveen, K., Heaps, A.D., et al. (2018). Genomic diagnostics within a medically underserved population: efficacy and implications. Genet. Med. *20*, 31–41.
31. Li, W.W., Alexandre, S., Cao, X., and Lee, A.S. (1993). Transactivation of the grp78 promoter by Ca^{2+} depletion. A comparative analysis with A23187 and the endoplasmic reticulum $Ca(^{2+})$-ATPase inhibitor thapsigargin. J. Biol. Chem. *268*, 12003–12009.
32. Bertolotti, A., Zhang, Y., Hendershot, L.M., Harding, H.P., and Ron, D. (2000). Dynamic interaction of BiP and ER stress transducers in the unfolded-protein response. Nat. Cell Biol. *2*, 326–332.
33. Petersen, O.H. (2014). Calcium signalling and secretory epithelia. Cell Calcium *55*, 282–289.
34. Ambudkar, I.S. (2014). Ca^{2+} signaling and regulation of fluid secretion in salivary gland acinar cells. Cell Calcium *55*, 297–305.
35. Trampert, D.C., and Nathanson, M.H. (2018). Regulation of bile secretion by calcium signaling in health and disease. Biochim Biophys Acta Mol. Cell. Res. *11*, 1761–1770.
36. Shibao, K., Hirata, K., Robert, M.E., and Nathanson, M.H. (2003). Loss of inositol 1,4,5-trisphosphate receptors from bile duct epithelia is a common event in cholestasis. Gastroenterology *125*, 1175–1187.
37. Martin, J., and Dufour, J.F. (2004). Cholestasis shuts down calcium signaling in cholangiocytes. Hepatology *39*, 248–249.
38. Futatsugi, A., Nakamura, T., Yamada, M.K., Ebisui, E., Nakamura, K., Uchida, K., Kitaguchi, T., Takahashi-Iwanaga, H., Noda, T., Aruga, J., and Mikoshiba, K. (2005). IP_3 receptor types 2 and 3 mediate exocrine secretion underlying energy metabolism. Science *309*, 2232–2234.
39. Michalak, M., Robert Parker, J.M., and Opas, M. (2002). Ca^{2+} signaling and calcium binding chaperones of the endoplasmic reticulum. Cell Calcium *32*, 269–278.
40. Milner, R.E., Famulski, K.S., and Michalak, M. (1992). Calcium binding proteins in the sarcoplasmic/endoplasmic reticulum of muscle and nonmuscle cells. Mol. Cell. Biochem. *112*, 1–13.
41. Baksh, S., and Michalak, M. (1991). Expression of calreticulin in *Escherichia coli* and identification of its Ca^{2+} binding domains. J. Biol. Chem. *266*, 21458–21465.
42. Koch, G., Smith, M., Macer, D., Webster, P., and Mortara, R. (1986). Endoplasmic reticulum contains a common, abundant calcium-binding glycoprotein, endoplasmin. J. Cell Sci. *86*, 217–232.
43. Van, P.N., Peter, F., and Söling, H.D. (1989). Four intracisternal calcium-binding glycoproteins from rat liver microsomes with high affinity for calcium. No indication for calsequestrin-like proteins in inositol 1,4,5-trisphosphate-sensitive calcium sequestering rat liver vesicles. J. Biol. Chem. *264*, 17494–17501.
44. Gilchrist, J.S., and Pierce, G.N. (1993). Identification and purification of a calcium-binding protein in hepatic nuclear membranes. J. Biol. Chem. *268*, 4291–4299.
45. Wada, I., Rindress, D., Cameron, P.H., Ou, W.J., Doherty, J.J., 2nd, Louvard, D., Bell, A.W., Dignard, D., Thomas, D.Y., and Bergeron, J.J. (1991). SSR alpha and associated calnexin are major calcium binding proteins of the endoplasmic reticulum membrane. J. Biol. Chem. *266*, 19599–19610.
46. Tjoelker, L.W., Seyfried, C.E., Eddy, R.L., Jr., Byers, M.G., Shows, T.B., Calderon, J., Schreiber, R.B., and Gray, P.W. (1994). Human, mouse, and rat calnexin cDNA cloning: identification of potential calcium binding motifs and gene localization to human chromosome 5. Biochemistry *33*, 3229–3236.
47. Lebeche, D., Lucero, H.A., and Kaminer, B. (1994). Calcium binding properties of rabbit liver protein disulfide isomerase. Biochem. Biophys. Res. Commun. *202*, 556–561.
48. Nakamura, K., Zuppini, A., Arnaudeau, S., Lynch, J., Ahsan, I., Krause, R., Papp, S., De Smedt, H., Parys, J.B., Muller-Esterl, W., et al. (2001). Functional specialization of calreticulin domains. J. Cell Biol. *154*, 961–972.
49. Mesaeli, N., Nakamura, K., Zvaritch, E., Dickie, P., Dziak, E., Krause, K.H., Opas, M., MacLennan, D.H., and Michalak, M. (1999). Calreticulin is essential for cardiac development. J. Cell Biol. *144*, 857–868.
50. Wanderling, S., Simen, B.B., Ostrovsky, O., Ahmed, N.T., Vogen, S.M., Gidalevitz, T., and Argon, Y. (2007). GRP94 is essential for mesoderm induction and muscle development because it regulates insulin-like growth factor secretion. Mol. Biol. Cell *18*, 3764–3775.
51. Kraus, A., Groenendyk, J., Bedard, K., Baldwin, T.A., Krause, K.H., Dubois-Dauphin, M., Dyck, J., Rosenbaum, E.E., Korngut, L., Colley, N.J., et al. (2010). Calnexin deficiency leads to dysmyelination. J. Biol. Chem. *285*, 18928–18938.
52. Konno, M., Shirakawa, H., Miyake, T., Sakimoto, S., Nakagawa, T., and Kaneko, S. (2012). Calumin, a Ca^{2+}-binding protein on the endoplasmic reticulum, alters the ion permeability of Ca^{2+} release-activated Ca^{2+} (CRAC) channels. Biochem. Biophys. Res. Commun. *417*, 784–789.

The American Journal of Human Genetics, Volume *103*

Supplemental Data

Bi-allelic *CCDC47* Variants Cause a Disorder Characterized by Woolly Hair, Liver Dysfunction, Dysmorphic Features, and Global Developmental Delay

Marie Morimoto, Helen Waller-Evans, Zineb Ammous, Xiaofei Song, Kevin A. Strauss, Davut Pehlivan, Claudia Gonzaga-Jauregui, Erik G. Puffenberger, Charles R. Holst, Ender Karaca, Karlla W. Brigatti, Emily Maguire, Zeynep H. Coban-Akdemir, Akiko Amagata, C. Christopher Lau, Xenia Chepa-Lotrea, Ellen Macnamara, Tulay Tos, Sedat Isikay, Michele Nehrebecky, John D. Overton, Matthew Klein, Thomas C. Markello, Jennifer E. Posey, David R. Adams, Emyr Lloyd-Evans, James R. Lupski, William A. Gahl, and May Christine V. Malicdan

SUPPLEMENTAL DATA

SUPPLEMENTAL NOTE: CASE REPORTS

Proband 1

The proband presented to the NIH Undiagnosed Diseases Program as a 5-year-old female of non-consanguineous, mixed Northern European and Native American descent with a complex medical history. She was born to a 30-year-old primagravida mother who carries a mosaic 46,XX, 47,XXX karyotype. Father and child both carried normal karyotypes. Pregnancy was complicated by polyhydramnios and slow fetal heart rates. Premature rupture of membranes at 30 weeks of gestation required preterm delivery by Caesarean section, but steroids and antibiotics were administered in a timely manner prior to delivery. The proband was a 1600-gram (75th %ile) infant with APGAR scores eight and nine, at one- and five-minutes respectively. On infant exam, she exhibited microcephaly, hypotonia, bilateral club foot deformities, and a patent ductus arteriosus. Her right foot was reduced at birth but the left required casting. Complete blood counts identified anemia during infancy, which resolved by 5 years of age. She was unable to breast or bottle feed and admitted to the NICU, where she was diagnosed with oral motor dyspraxia and severe gastroesophageal reflux (GERD). Due to microcephaly and developmental concerns neuroimaging was ordered. At 6 weeks of age, oral feedings remained recreational and nasogastric supplementation proved insufficient to support weight gain. She required Nissen fundoplication with gastrostomy tube (G-tube) placement. She did well with high fiber supplement PediaSure Formula and grew along the 5th percentiles until 8 months of age, after which growth accelerated.

Survey imaging around 2 years old revealed mild, generalized osteopenia. Luckenschadel ("copper beaten") calvaria suggested increased intracranial pressures. Lumbar vertebrae were

notably elongated in the craniocaudal dimension, however with uniform marrow and disk spaces. The tip of the conus projected to the upper L1 level. A fibrolipoma of the filum terminale tethered to the posterior aspect of the thecal sac at L4. There was slight increase in the lipomatous tissue within the epidural space in the upper sacral regions but no intrathecal lipoma or nerve root displacement. She underwent partial L1-partial L2 laminectomy and sectioning of fatty phylum terminale to preempt the possible loss of bladder-bowl-lower extremity function with age. She demonstrated incomplete ossification at the pubic rami, bilateral cox valga, with mild tibial bowing. She continues to experience chronic bilateral hip subluxation and dislocation with spontaneous reductions.

The proband began to demonstrate episodes of nighttime oxygen desaturations from a daytime baseline of 93% to as low as 68%. Procedural sedations with fentanyl and propofol demonstrated similar oxygen desaturations. Sleep studies did not identify obstructive or central apneic pauses, but she was referred for tonsillectomy and adenoidectomy at 11 months of age for obstructive sleep apnea. Sleep studies also identified advanced circadian phase and fragmented sleep patterns. Specifically, electroencephalography background consisted of delta and theta rhythms, distributed symmetrically over the hemispheres. Chewing and rocking artifacts were noted. Occasional dominant 3-4 Hz rhythms are seen but without focalities or epileptiform charges.

She began to have irregular stooling patterns at 2 years of age. She had decreased lower gastrointestinal motility and took standard lactose free formulas on an unvarying diet. Feeding and swallow evaluation identified feeding resistance secondary to oral hypersensitivity and sensory defensiveness. She experienced a significant gastrointestinal bleed following G- tube replacement. The tissue around the stoma was notably friable and bled easily. Recurrent emesis

prompted an endoscopic evaluation. Her esophagus and duodenum were normal. Her stomach demonstrated focal erythema in several areas along the greater curvature with a small ulceration below the G-tube, but no active bleed was identified. Lower endoscopy was negative. Evaluation for inflammatory bowel disease was negative. The bleed was later attributed to a cholelith tearing of the bile ducts.

Starting around 3 years of age, the proband experienced an episode of pancreatitis with liver inflammation. She had recurrent steatorrhea and low fecal elastase levels, but no history of hyperbilirubinemia or acholic stools. The process was considered to be due to biliary microlithiasis. The common bile duct was normal on ultrasound and endoscopic retrograde cholangiopancreatography, but multiple smooth surface, multifaceted grey-black cholesterol stones were identified. Severe pruritus persisted despite treatment with bile salts leaving the proband uncomfortable most hours of the day. Cholecystectomy failed to resolve the problem and she progressed to recurrent hospitalizations for similar episodes of pancreatitis. She failed all treatments to control symptoms of her severe pruritus and urticaria. Evaluation for primary biliary cholangitis and autoimmune hepatitis were negative. Neither endoscopic retrograde cholangiopancreatography nor subsequent magnetic resonance cholangiopancreatography identified pancreas divisum. Pancreatic ducts were of normal caliber and signal. Liver biopsies revealed portal-based septal fibrosis, stage two to three, mild sinusoidal dilation, and increased copper deposition, without stainable iron. The liver changes were considered related to pancreatic irritability, given the 2+ distribution of copper within the centrizonal hepatocytes. Biliary obstruction and Wilson's disease characteristically presents with portal-based and zonal-based distributions, respectively. The copper present in the liver biopsy is furthermore suggestive of an independent metabolic process. She was otherwise diagnosed with exocrine pancreatic

insufficiency. On imaging, there was no significant scarring or calcification of the pancreas. She showed only large dilated, gas filled bowel loops. She had never had a period of significant cholestasis, although she had elevations in direct bilirubin.

She had no hearing difficulties, but a history of recurrent otitis media with tympanic perforations. She required bilateral tympanostomy tubes by 3 years of age. The inner ear structures are grossly unremarkable, however there was suspected superior semicircular canal dehiscence. She experienced a parainfluenza type 2 pneumonia at 4 years old. All immunizations were up to date. Family history was significant for three spontaneous abortions subsequent to the birth of the proband and developmental delays with learning difficulties in one paternal cousin. Karyotyping and signature microarray returned inconclusive. She was managed on daily regimens of polyethylene glycol, oral pancrelipase supplements, ursodiol, loratadine, famotidine, and triamcinolone acetonide cream. She was given albuterol, nystatin, ofloxacin otic drops, and ibuprofen as needed. With bladder distention, there was notably posterior-inferior extrinsic indentation evident. She had no bladder problems.

At 5 years old, height remained at the 50th percentile, and weight between the 15th and 20th percentiles. She exhibited microcephaly, brachycephaly, and positional plagiocephaly. Her hair was sparse, curly, and woolen. She had low-set ears, symmetrical but coarse facies with midface hypoplasia, hypertelorism, long eyelashes, a downturned mouth, and a small nose. She had roving eye movements with ptosis, but extraocular movements were intact, without nystagmus. On dilated ophthalmologic examination, she had a normal macula, disc, and vessels. Both optic nerves were pink. She had astigmatism, hyperopia, and cortical visual impairment. Formal speech and language pathology evaluation around two years old identified a receptive and expressive language delay of over 50% for age. She remains significantly developmentally

delayed. She looked around, especially at bright lights, but did not make eye contact or look at specific objects for extended periods of time. Hearing was intact. She seemed to be able to hear and localized sounds well. Proband remained unable to follow commands. She made noises, but no specific words. She remained constantly moving, writhing, and moaning.

She demonstrated thick lips, a small chin, an underbite with dental crowding. Her palate elevated, and her tongue lay at the midline, without fasciculations. She had a normal pharynx. She demonstrated a loss of lumbar lordosis, but no other spinal abnormality. She demonstrated both truncal and appendicular hypotonia with poor head control. She had frog leg posturing when lying down. She moved both arms and legs equally well. She did not however hold objects, bear weight, or sit up without support. She could roll over and used a wheelchair and a series of standers allowing various postures. She expressed satisfaction with massage of her arms and legs. Deep tendon reflexes were suppressed throughout and especially in the lower extremities. She has arthrogrypotic third digits, and bilateral but asymmetrical hypoplasia of the fifth digits. Her left fifth digit is missing the majority of the distal phalanx and the entirety of the nail. Extremities are otherwise without clubbing, cyanosis, or edema. She demonstrated dry skin, mild hypertrichosis of the trunk, and multiple healing abrasions to upper extremities. She was without jaundice or petechiae. Genital exam was significant for clitoral hyperplasia and a small sacral dimple. On auscultation, there was clear S1, S2, regular rate and rhythm with a III out of VI systolic ejection murmur at the left sternal border, but no other rubs or gallops. Her chest was narrow, but the point of maximal impulse was not displaced. Her lungs were clear to auscultation without rales, rhonchi, wheeze, or accessory muscle recruitment. Gastrostomy stoma and cholecystectomy laparoscopy sites were well healed. Her abdomen was non-tender and non-distended with positive bowel sounds. She had hepatosplenomegaly.

CT scans of the temporal lobes identified clear fluid in right middle ear and mastoid air cells as well as a completely opacified left middle ear and left mastoid air cells with bony thinning along the posterior aspect of the mastoid bone. Subsequent brain MRI confirmed several abnormalities of the skull. She had an osteopenic, Luckenschadel skull with brachycephaly with flattening along the right occipital and posterior parietal regions, left to right asymmetry, and low-set ears with the left lower than the right. The brain conformed to the shape of the skull, but the splenium of the corpus callosum had a minor posterior thinning; this was not associated with colpocephaly. The cortical sulci were mildly enlarged, suggesting hypoplasia in the absence of neuromigration anomalies or other congenital malformations in the brain. There was decreased hypointense myelination on the frontal region and anterior limb of the internal capsules relative to age-matched controls. The corpus callosum was myelinated but has an atypical inverted U-shape contour. The pituitary and suprasellar regions were normal. Cranial nerves seven and eight were intact, and inner ear structures and cranial nerves five and six were intact. There was no neuromigration or focal thickening of the cerebellar cortex. There was relative hypoplasia of the nasal bones. Visible intracerebral vasculature and dural sinuses were normal. There was a low position of the torcula without cerebellar exotropia. There was mild prominence of the extra-axial CSF spaces, including the Sylvian fissure, and mild prominence of the third ventricle. No abnormalities of neural migration were identified. The degree of myelination appeared to be appropriate for the proband's age and had significantly progressed when compared to the exam at 17 months of age. However, the terminal zones remained incomplete and amyelinated. MRS identified reduced N-acetyl aspartate levels.

Proband 3

Proband 3 was an Old Order Amish female first seen at The Community Health Clinic (Topeka, IN) at the age of 8 years. She had been followed at Children's Mercy Hospital (Kansas City, MO) for several years with no confirmed diagnosis. She was born to a 33-year-old G10P7A2 mother. There were no major complications during the pregnancy. The mother reported that she measured small and that the movements were slow and less frequent compared to her previous pregnancies. The proband was born at 38 weeks of gestation via normal spontaneous vaginal delivery (NSVD) at home with the presence of a midwife. At birth, the umbilical cord was small and "shriveled", but was three-vessel. The proband was a 2070-gram (<3rd %ile) infant, consistent with small for gestational age (SGA). She was very pale at birth, did not cry for 10-15 minutes, and required extensive suctioning. She was transported to Wright Memorial Hospital (Trenton, MO) where she was placed on oxygen for 12-24 hours. Newborn screening was normal. She was also noted to have a flat right occiput and bilateral clubfoot and hip dysplasia at birth.

Developmentally, her mother reported that the baby was not as responsive as normal at 3 weeks. At 3 months of age, she was diagnosed with failure to thrive (FTT) at which time she had a G-tube placed and she was placed on PediaSure. At 8 years of age, she was able to roll onto her side, but not stomach to back or vice versa. She was unable to grasp objects. The proband was non-verbal, but she made some sounds where her parents could tell if she was happy or upset. She was incontinent of urine and stool. The proband had started to attend a public school that has a program for children with special needs three full days per week.

Her physical examination revealed she was small for her age at 8 years old and she had several dysmorphic features. Facial dysmorphic features included microcephaly with plagiocephaly, bitemporal narrowing, arched eyebrows, coarse facial features, hypertelorism,

epicanthal folds, bulbous nasal tip, wide mouth with high palate and widely spaced teeth, exotropia, and curly coarse hair. She also had a short neck, small hands and feet, dystrophic nails, abnormal chubby toes, overlapping third and fourth toes, genu valgum, scoliosis, and clitoral hyperplasia. Neurologically, she was non-verbal and had severe delays, generalized hypotonia, muscle atrophy, ptosis, and hyperreflexia; she had no eye contact or tracking. The proband had a history of behavioral issues including bruxism, self-mutilation, screamed and hit herself, and easy agitation; she has shown improvement on 0.25 mg Risperadol BID as she was happy, calm, laughing, and smiling. Her skin showed scarring from self-mutilation on her upper and lower extremities; less self-mutilation was reported upon treatment.

Her gastroenterological findings included a history of feeding issues, FTT, GERD, chronic diarrhea, and liver dysfunction. Her abnormal liver function tests (LFTs) included elevated alanine transaminase (ALT, 44-343 U/L), aspartate aminotransferase (AST, 100-202 U/L), alkaline phosphatase (ALP, 209 U/L), total bilirubin (1.4-1.5 mg/dL), and direct bilirubin (0.4-0.5 mg/dL). Work-up for liver dysfunction showed that there was no evidence for autoimmune hepatitis, Wilson's disease, alpha-1 antitrypsin deficiency, or hemochromatosis. She also tested negative for celiac. Abdomen ultrasound revealed she had mild splenomegaly and a prominent left hepatic lobe; her liver Doppler ultrasound was normal. Her pruritus had substantially improved with 0.5 packet cholestyramine BID, though she is still itching. She was found to have iron, zinc, and vitamin D deficiency and was started on supplementation.

Evaluation of her other systems showed she had immunological, endocrinological, and pulmonary findings. She has had a history of recurrent infections including frequent urinary tract infections, otitis media, and upper respiratory tract infections, and she had been found to have a TLR signaling defect. The recurrent infections had been treated with IVIG since the age of 2

years 9 months, however the infusions were discontinued at the age of 5 as IgG levels remained within normal. Evaluation of her endocrine system showed that she had transient central hypothyroidism and vitamin D deficient rickets. She also had asthma, chronic respiratory insufficiency, sleep apnea, and sleep disturbances.

A brain MRI study at the age of 2 months showed mild hypoplasia of the cerebellum and mild prominent CSF space surround the left cerebellar hemisphere and inferior to the cerebellar vermis. There was no evidence of intracranial hemorrhage, masses, or acute ischemic changes. She had had a history of seizures and EEG abnormalities of which the former has resolved; no repeat EEGs have been performed.

All diagnostic and genetic testing prior to whole exome sequencing had been unrevealing. The proband had a normal karyotype and SNP microarray. Comprehensive sequencing was performed for Noonan, LEOPARD, cardiofaciocutaneous, and Costello syndromes at GeneDx (*KRAS*, *HRAS*, *PTPN11*, *NRAS*, *MAP2K1*, *RAF1*, *SOS1*, *SHOC2*) for which she tested negative. Testing for congenital disorders of glycosylation (CDGs), including N-glycan structural analysis and carbohydrate deficient transferrin, was negative.

Her mother and father were non-consanguineous Old Order Amish from Kansas and Iowa, respectively. The proband had three healthy brothers (3: II-1, 3: II-2, and 3: II-5) and 2 healthy sisters (3: II-4 and 3: II-7), however there have been two miscarriages at 6 and 8 weeks of gestation. One brother (3: II-3) passed away at 3.5 months old due to aspiration pneumonia; he had unilateral cleft lip and palate, FTT, breathing problems, and dark curly hair similar to the proband. Another brother (3: II-6) was a stillborn at 7 months of gestation; he had bilateral cleft lip and palate and dark curly hair similar to the proband. A maternal uncle passed away at 9 weeks old due to kidney failure; he was reported to have similar dark curly hair.

Proband 4

Proband 4 was an Amish female first seen at The Community Health Clinic (Topeka, IN) at the age of 6 years 6 months. She was born to a 22-year-old G1P0 mother. The mother had a bicornuate uterus, but she had an uncomplicated pregnancy until 7 months of gestation when the fetus was noted to have bradycardia. Her mother was treated with steroids due to possible premature labor. During the pregnancy, the mother smoked approximately 5 cigarettes per day and she had 2-3 alcoholic beverages approximately 3 times per week for first 4 weeks of pregnancy. She denied drug use. Proband 4 was born at 41 weeks of gestation via emergency Caesarean section at Goshen General Hospital. Her birth weight was 2835 grams (6 lbs 4oz), her length was 47 cm, and her head circumference was 33 cm. At birth, she was transferred to the NICU at Memorial Hospital (South Bend, IN) for 5 days due to episodes of oxygen desaturation and poor feeding. At 1 year 6 months, she had a G-tube placed due to FTT. At 2 years 6 months, she had a tonsillectomy and ear tubes due to recurrent otitis media. At 3 years, she had surgery on her left foot to release and lengthen her tendon. At 7 years, a hiatal hernia repair and Nissen fundoplication were performed. She was placed on PediaSure Enteral Formula with Fiber.

Physical examination showed the proband had microcephaly, bitemporal narrowing, coarse features, bushy eyebrows, synophrys, full lips, high arched palate, small widely spaced teeth, and curly red hair. She also had a short neck, pectus excavatum, hypoplastic nipples, hypermobile joints, small feet with overlapping toes, bilateral congenital talipes equinovarus, and hip dysplasia. Neurologically, the proband was severely globally developmentally delayed with hypotonia, poor head control, muscle atrophy, and hyperreflexia; she had no eye contact or tracking. She was non-verbal but would answer “yah” and also made sounds sometimes like

"ma" and "da". She also had a history of behavioral issues including bruxism, self-mutilation, and hitting herself or clapping when excited. Her skin showed scarring from self-mutilation and she had multiple scratches from itching. A vision examination revealed that she had hyperopia, pinguecula, hypertropia, and bilateral ptosis. She tested normal for hearing.

The proband's gastroenterological findings included a history of feeding issues, FTT, GERD, chronic diarrhea, and liver dysfunction. Her abnormal LFTs included elevated ALT (25-69 U/L), AST (22-62 U/L), and ALP (308 U/L). Her recent bile acids profile at 10 years of age on cholestyramine showed she had high cholic acid (11.2 μmol/L), chenodeoxycholic acid (5.9 μmol/L), and total bile acids (19.0 μmol/L). A gallbladder ultrasound at 9 years of age showed that she had a single large gallbladder stone without secondary evidence of acute cholecystitis. She was placed on 0.5 packet cholestyramine BID as well as Bactrim (sulfamethoxazole-trimethoprim), Dilaudid (hydromorphone), and Tylenol (acetaminophen) for her severe pruritus. She showed improvement on cholestyramine.

A brain MRI at showed that she had minimal prominence of the cerebral sulci and minimal ventricular enlargement. MR spectroscopy showed she had global white matter paucity. There was no evidence of a demyelinating or dysmyelinating condition or focal insult. Her overlying cortical thickness and sulcation were normal. Although her EEG was abnormal, these abnormalities were not associated with clinical seizure activity.

All diagnostic and genetic testing prior to whole exome sequencing had been unrevealing. The proband had a normal karyotype and SNP microarray, though SNP array showed a number of regions of allelic homozygosity (ROH) that were larger than 5 Mb in size with a total of 57.2 Mb of ROH. Targeted testing for Byler disease (*ATP8B1*), ITCH deficiency (*ITCH*), and GM3 synthase deficiency (*ST3GAL5*); all of which were negative. Testing for Rett

syndrome (*MECP2*) and Prader-Willi syndrome were also negative. Mitochondrial DNA content testing on muscle and liver biopsies, electron transport chain enzyme analysis on skeletal muscle, as well as mitochondrial DNA sequencing were all normal. Testing for CDGs was negative. A cholestasis panel (EGL Genetics, Tucker, GA) detected one pathogenic variant in *POLG* (c.[752C>T;1760C>T], p.[(Thr251Ile;Pro587Leu)]), however a second reportable variant was not identified.

Her mother and father were non-consanguineous Amish from Oklahoma/Indiana and Indiana, respectively. The proband had three healthy siblings (4: II-2, 4: II-3, and 4: II-4) and she is the only affected individual in her family.

SUPPLEMENTAL FIGURES

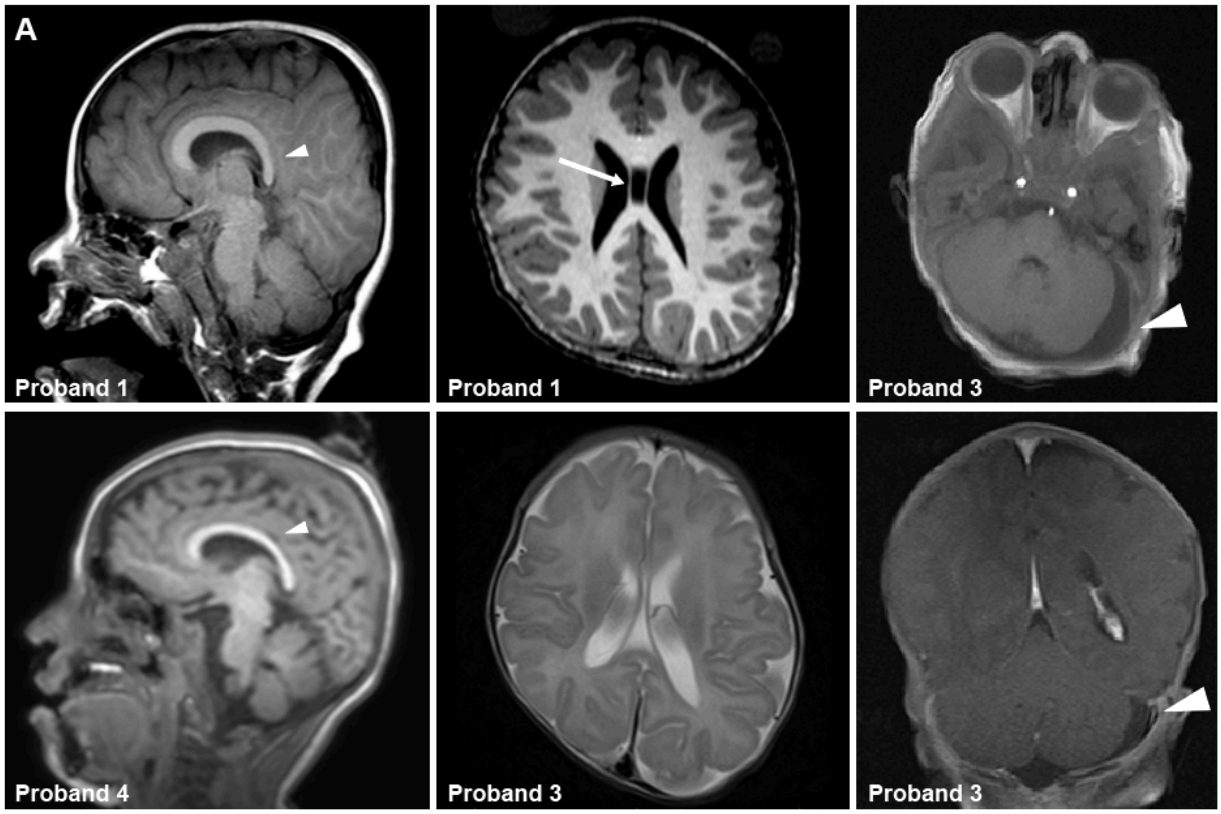

Figure S1. Radiographs of individuals with bi-allelic loss-of-function *CCDC47* variants. (A) Brain MRIs of Probands 1, 3, and 4. Note the thin corpus callosum in Probands 1 and 4 (small white arrowheads in the sagittal plane, left panels), cerebral atrophy in Probands 1 and 3 (transverse plane, center panels), and mild prominence of the third ventricle in Proband 1 (white arrow in the transverse plane, center upper panel). There is a stable mild prominence of cerebrospinal fluid surrounding the left cerebellar hemisphere in Proband 3 (large white arrowheads in the transverse and coronal planes, right panels). (B) An x-ray of the lower extremities of Proband 2 shows evidence of osteoporosis.

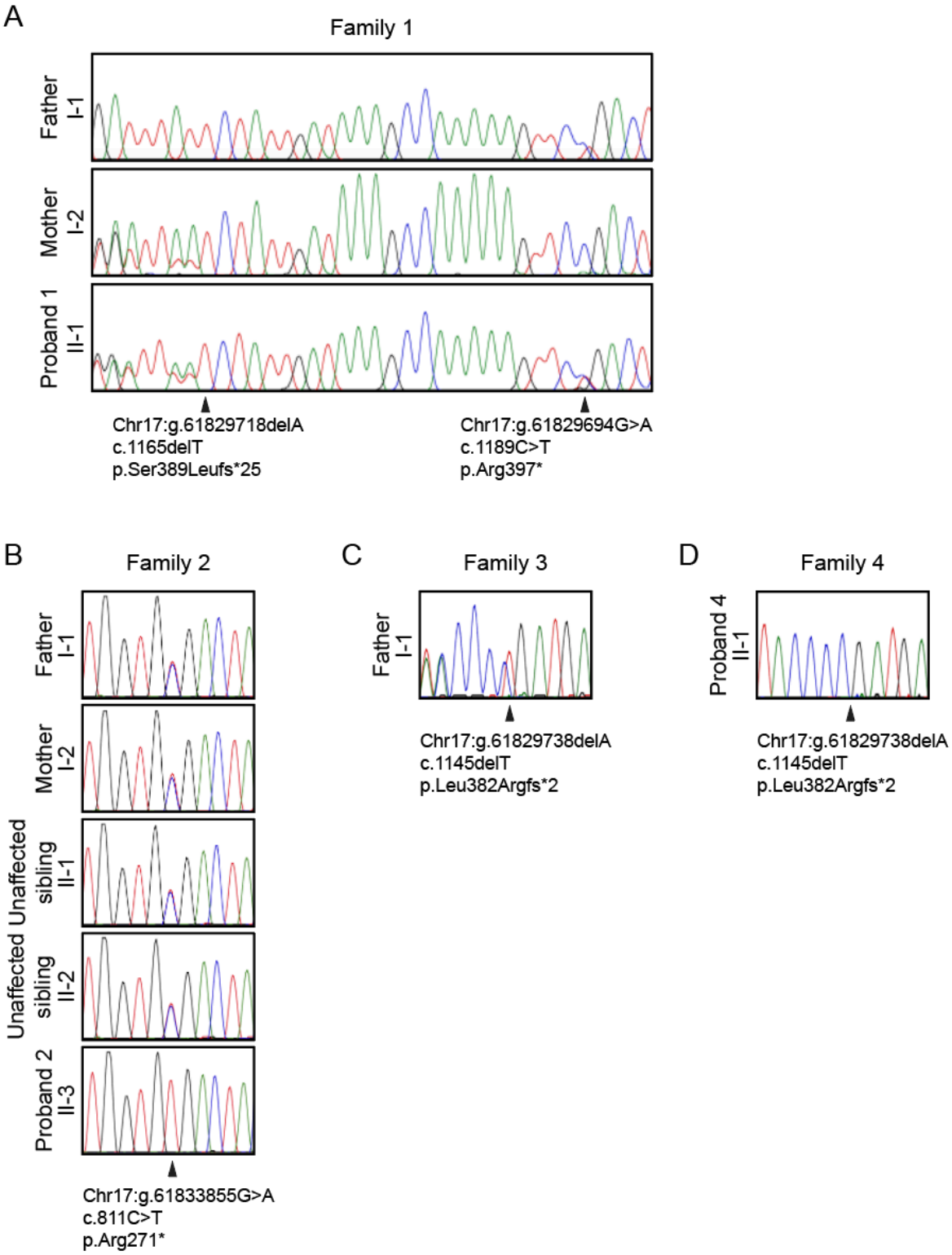

Figure S2. Sanger sequencing chromatograms of the four probands with bi-allelic variants in *CCDC47* (NM_020198.2). (A) Proband 1 has a paternally inherited c.1189C>T variant and a maternally inherited c.1165delT variant in *CCDC47*. (B) Proband 2 has a homozygous c.811C>T variant in *CCDC47*. Probands 3 (C) and 4 (D) have a homozygous c.1145delT variant in *CCDC47*.

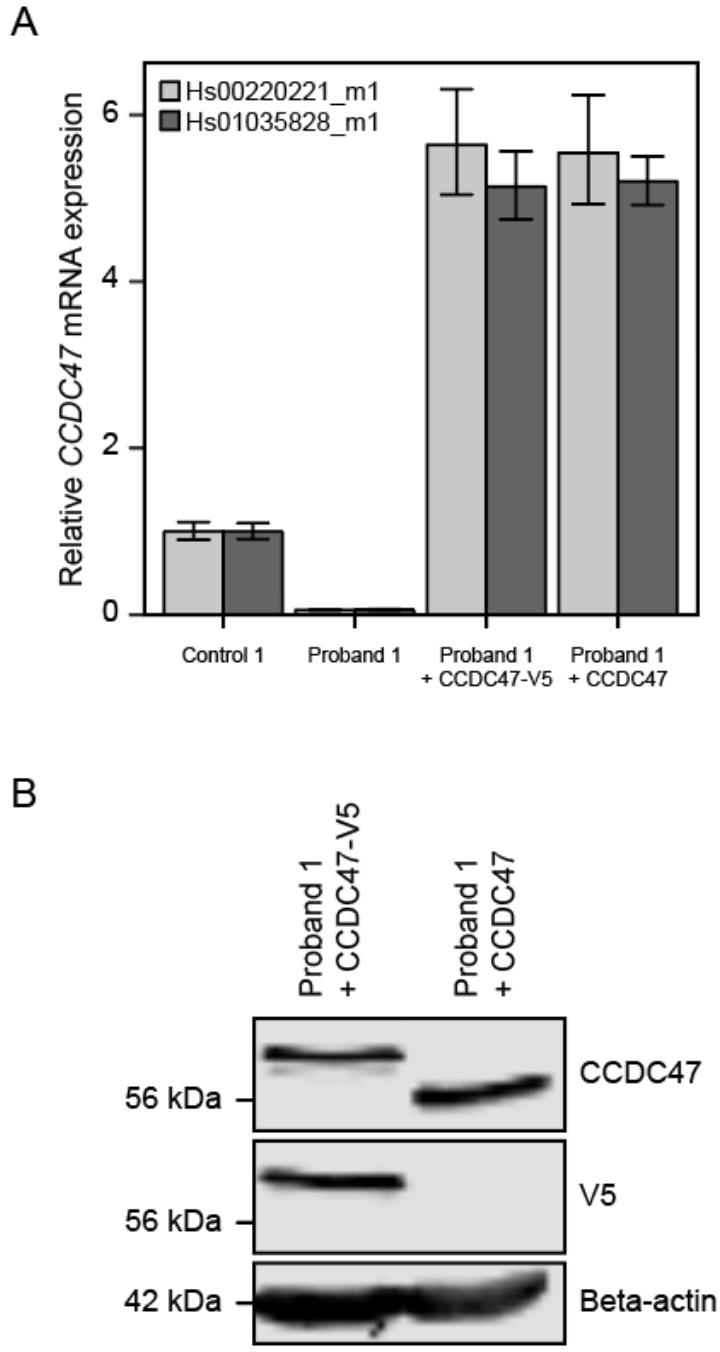

Figure S3. Wild type *CCDC47* mRNA was overexpressed in Proband 1 fibroblasts by lentiviral transduction of pLenti6.3-CCDC47-V5 and pLenti6.3-CCDC47. (A) Relative *CCDC47* mRNA expression analysis by TaqMan assay in unaffected control, Proband 1, and Proband 1 rescued fibroblasts expressing V5-tagged and untagged *CCDC47* mRNA. Data are presented as the mean of 3 technical replicates relative to control 1. Expression of *HPRT1* and *POLR2A* were used as internal controls to normalize gene expression; error bars represent one standard deviation. (B) CCDC47 protein level analysis by western blot in rescued Proband 1 fibroblasts expressing V5-tagged CCDC47 and untagged CCDC47.

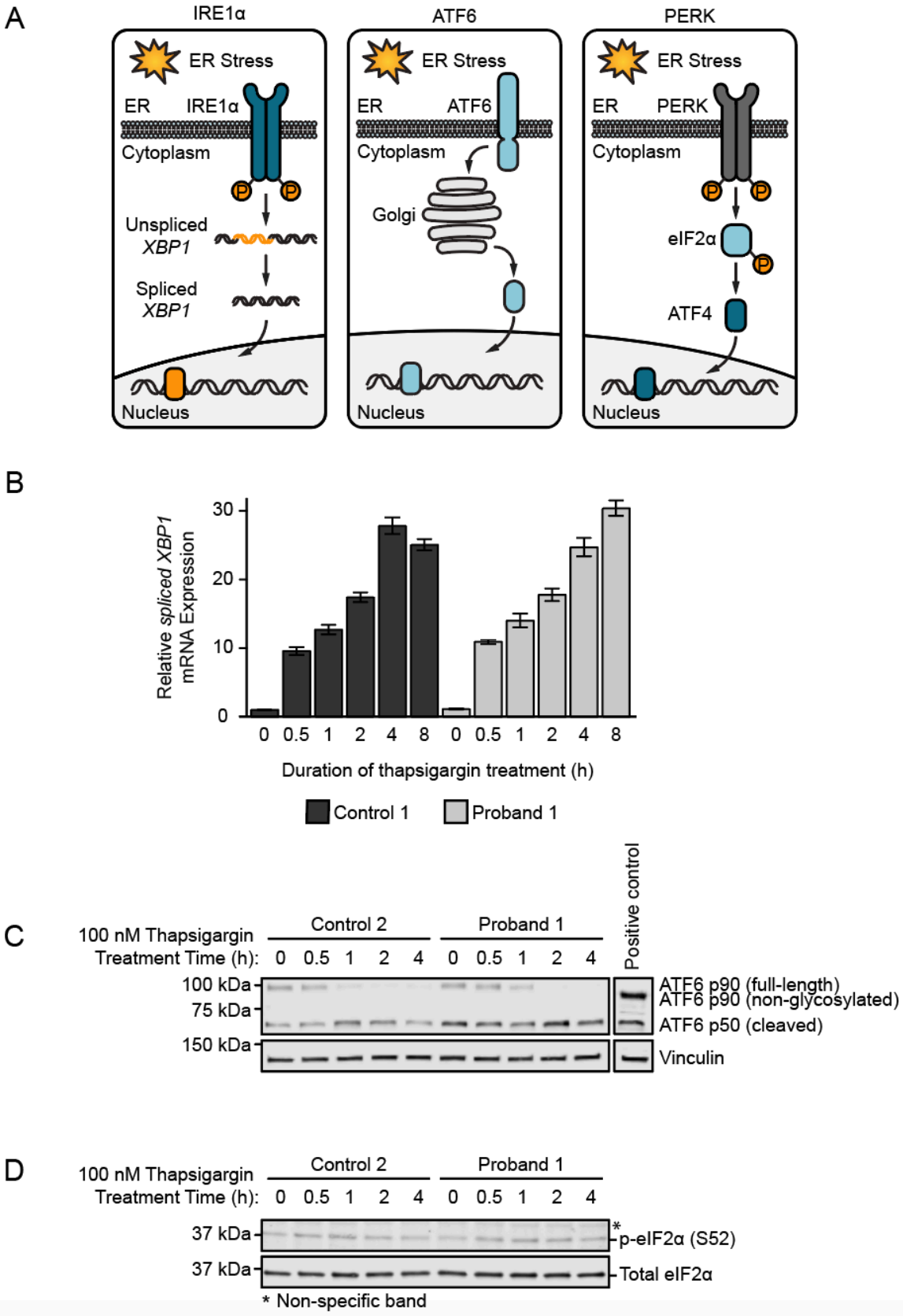
A
IRE1α
ATF6
PERK
ER Stress
ER
IRE1α
ATF6
PERK
Cytoplasm
Unspliced XBP1
Spliced XBP1
Golgi
eIF2α
ATF4
Nucleus
B
Relative spliced XBP1 mRNA Expression
30
20
10
0
0 0.5 1 2 4 8 0 0.5 1 2 4 8
Duration of thapsigargin treatment (h)
Control 1
Proband 1
C
100 nM Thapsigargin
Treatment Time (h):
Control 2
Proband 1
0 0.5 1 2 4 0 0.5 1 2 4
Positive control
100 kDa
75 kDa
150 kDa
ATF6 p90 (full-length)
ATF6 p90 (non-glycosylated)
ATF6 p50 (cleaved)
Vinculin
D
100 nM Thapsigargin
Treatment Time (h):
Control 2
Proband 1
0 0.5 1 2 4 0 0.5 1 2 4
37 kDa
37 kDa
*
p-eIF2α (S52)
Total eIF2α
* Non-specific band

Figure S4. The unfolded protein response (UPR) is comparably initiated in Proband 1 fibroblasts compared to unaffected control. (A) Schematic of the three arms of the UPR including the IRE1α, ATF6, and PERK pathways. Endoplasmic reticulum (ER) stress leads to IRE1α phosphorylation and subsequent splicing of *XBP1* that is translated into a transcription factor which is translocated into the nucleus (left panel) and/or the cleavage of ATF6 into a transcription factor which is translocated into the nucleus (center panel) and/or the phosphorylation of PERK and eIF2α that lead to the activation of ATF4 transcription factor which is translocated into the nucleus (right panel) to induce the transcription of UPR target genes. (B) *XBP1* splicing assay by quantitative PCR analysis to assess the IRE1α pathway upon ER stress with 100 nM thapsigargin for 0, 0.5, 1, 2, 4, or 8 hours in unaffected control and Proband 1 fibroblasts. Data are presented as the mean of 4 technical replicates relative to 0 hours for each sample. Expression of *TBP* was used as the internal control to normalize gene expression; error bars represent one standard deviation. (C) Cleaved ATF6 (p50) protein levels were analyzed by western blot to assess the ATF6 pathway upon ER stress with 100 nM thapsigargin for 0, 0.5, 1, 2, or 4 hours. The positive control is unaffected control fibroblasts treated with 10 μg/ml tunicamycin for 16 hours; the non-glycosylated ATF6 p90 is observed as tunicamycin is an inhibitor of glycosylation and the cleaved ATF6 p50 is observed as expected. (D) Phosphorylated eIF2α (S52) protein levels were analyzed by western blot to assess the PERK pathway upon ER stress with 100 nM thapsigargin for 0, 0.5, 1, 2, or 4 hours.

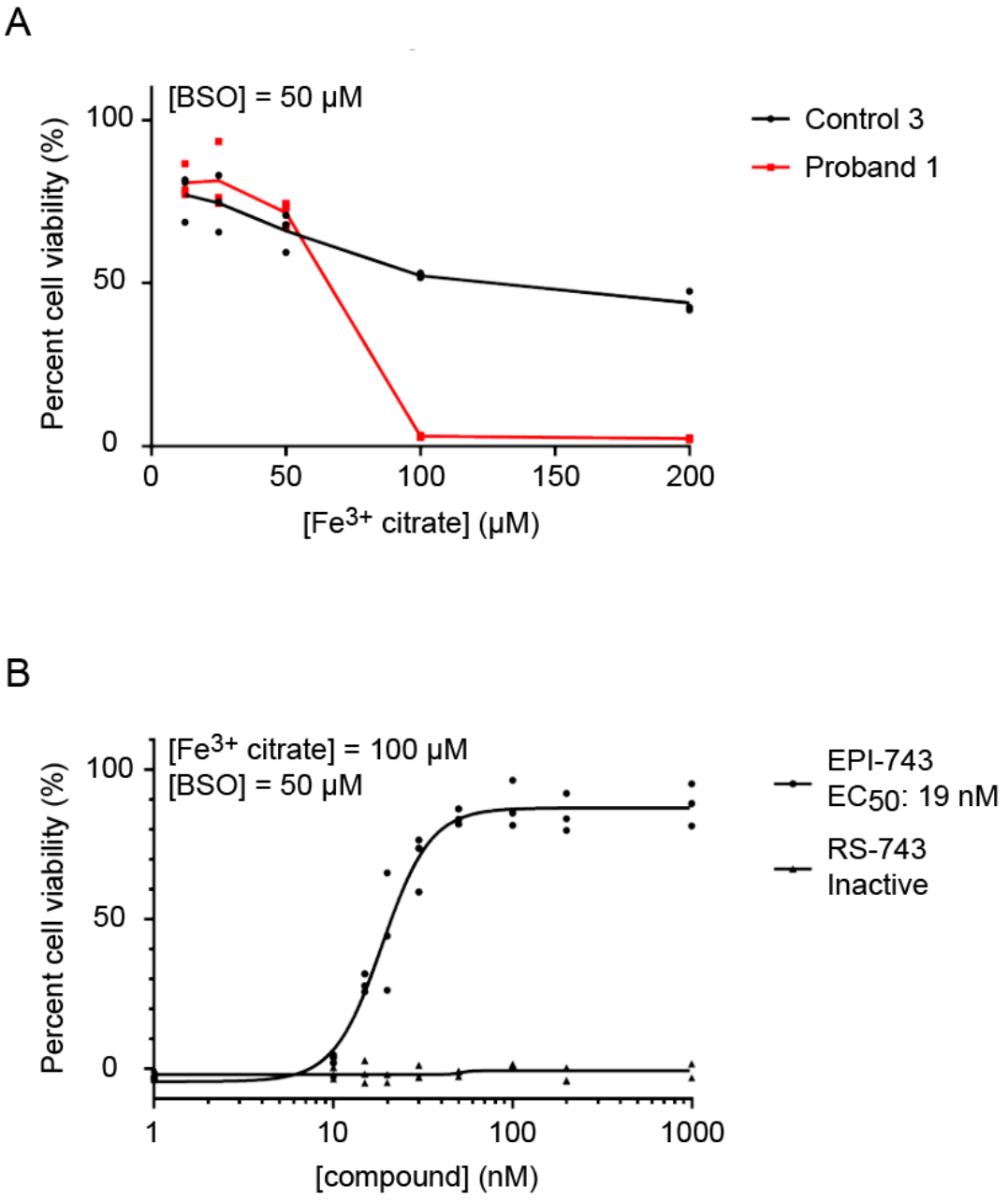

Figure S5. Proband 1 fibroblasts have increased susceptibility to oxidative stress and the antioxidant compound EPI-743 rescues the fibroblasts from oxidative stress-induced cell death. (A) Proband 1 fibroblasts have increased susceptibility to oxidative stress as shown by increased cell death upon treatment with a fixed concentration of 50 µM of the glutathione synthesis inhibitor L-buthionine-(*S*,*R*)-sulfoximine (BSO) for 48 hours and increasing concentrations of Fe^{3+} citrate compared to unaffected control fibroblasts. (B) Treatment with increasing concentrations of the antioxidant compound EPI-743 or its redox-silent analog RS-743 demonstrates the rescue of Proband 1 fibroblasts from oxidative stress-induced cell death under 100 µM Fe^{3+} citrate and 50 µM BSO challenge conditions. Abbreviations: EC_{50}, half maximal effective concentration.

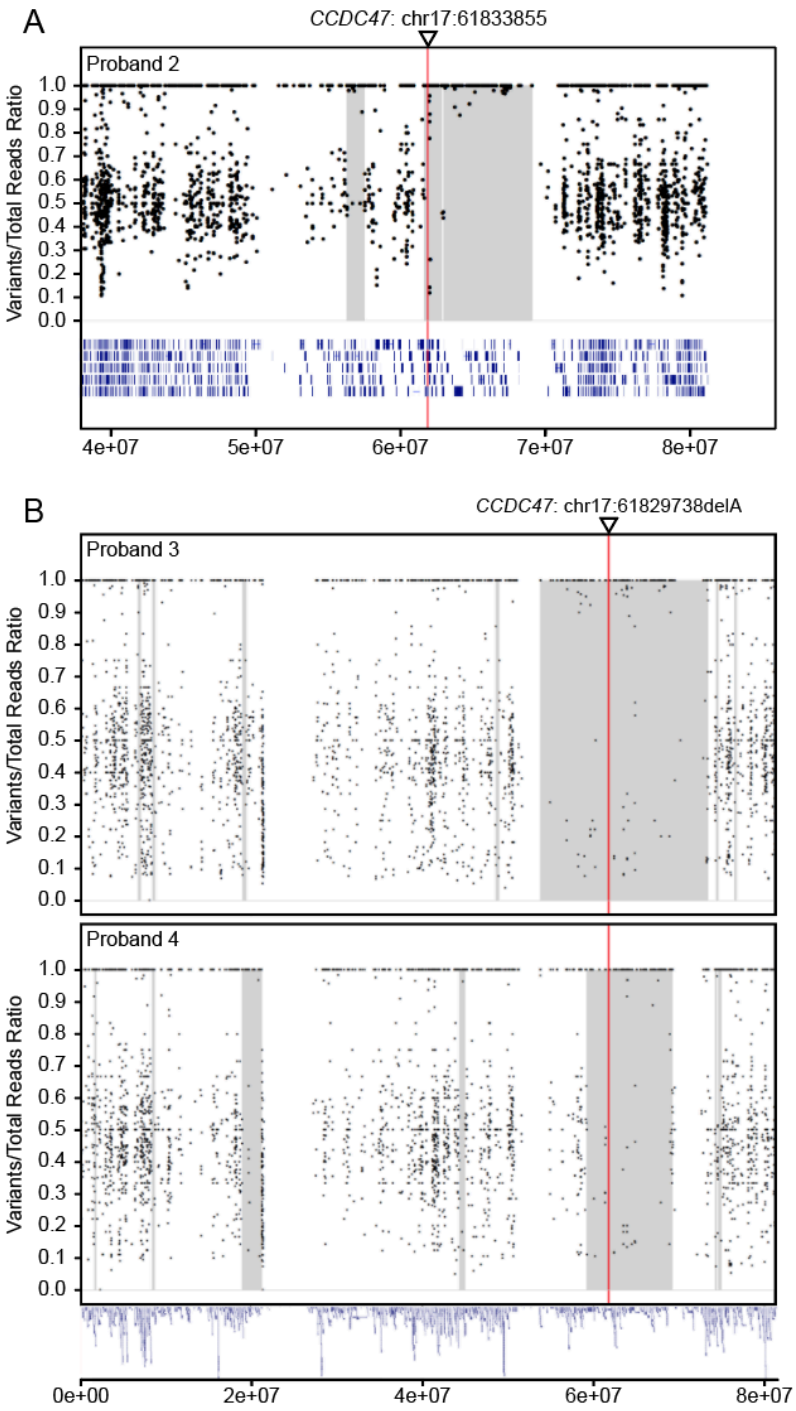

Figure S6. Absence of heterozygosity (AOH) analyses for Probands 2, 3, and 4. The homozygous variant NM_020198.2:c.811C>T in Proband 2 is located within a region of AOH. (B) The homozygous frameshift variant NM_020198.2:c.1145delT in Probands 3 and 4 is located within a region of AOH. The regions of AOH (grey blocks) were determined by B-allele frequency calculated by the ratio of variant to total reads from WES data at each base position. The homozygous *CCDC47* variants in each individual are located within a region of AOH on Chromosome 17, marked by a red line.

SUPPLEMENTAL TABLES

Table S1. TaqMan gene expression assays used in this study.

Gene	Assay ID	Exon Boundary
CCDC47	Hs01035828_m1	8-9
CCDC47	Hs00220221_m1	12-13
HPRT1	Hs02800695_m1	2-3
POLR2A	Hs00172187_m1	1-2
TBP	Hs00427620_m1	2-3 for NM_001172085.1 3-4 for NM_003194.4

Table S2. Oligonucleotide primers used in this study.

Primer Name	**Primer Sequence (5′ to 3′)**	**Application**
XBP1(S)-F	TGCTGAGTCCGCAGCAGGTG	*XBP1* splicing assay
XBP1(S)-R	GCTGGCAGGCTCTGGGGAAG	*XBP1* splicing assay
TBP-F	CCAAGAGTGAAGAACAGTCCAG A	*XBP1* splicing assay
TBP-R	ACTTCACATCACAGCTCCCC	*XBP1* splicing assay
CCDC47-cloning-F	CACCATGAAAGCCTTCCACACT	PCR amplification of *CCDC47* ORF for cloning
CCDC47-cloning-stop-R	TTACATGGCTTTCACTTTGATTTG TT	PCR amplification of *CCDC47* ORF (with stop codon) for cloning
CCDC47-cloning-no stop-R	GCCCATGGCTTTCACTTTGAT	PCR amplification of *CCDC47* ORF (without stop codon, glycine) for cloning
M13(-20)-mod-F	GTTGTAAAACGACGGCCAGTC	Sequence validation for pENTR-CCDC47
CCDC47-M13-R	CCTCCTGGGTATCTGCATCTTC	Sequence validation for pENTR-CCDC47
CCDC47-Inner-F	ACCACTGTGGAGTTGGAAGG	Sequence validation for pENTR-CCDC47 and pLenti6.3-CCDC47
CCDC47-Inner-R	AAAGAGTCCGGCAGTCCATA	Sequence validation for pENTR-CCDC47 and pLenti6.3-CCDC47
CCDC47-T7-F	GGAAAGCCTTGGTGCGACTA	Sequence validation for pENTR-CCDC47
T7-mod-R	CATGTAATACGACTCACTATAGG GGAT	Sequence validation for pENTR-CCDC47
CMV-mod-F	CAAATGGGCGGTAGGCGT	Sequence validation for pLenti6.3-CCDC47
CCDC47-CMV-R	CCTCCTGGGTATCTGCATCTTC	Sequence validation for pLenti6.3-CCDC47
CCDC47-V5-F	ATTTGCTGTTGGCACACGGA	Sequence validation for pLenti6.3-CCDC47
V5-R	ACCGAGGAGAGGGTTAGGGAT	Sequence validation for pLenti6.3-CCDC47

Abbreviations: F, forward; R, reverse.

Table S3. Antibodies used in this study.

Antibody	Application	Dilution	Catalog No.	Company
anti-β-actin	WB	1:50,000	ab6276	Abcam
anti-ATF6	WB	1:1,000	24169-1-AP	Proteintech
anti-calnexin	IF	1:100	MAB3126	EMD Millipore
anti-CCDC47 (C-terminus)	WB	1:250	HPA029674	Sigma-Aldrich
anti-CCDC47 (C-terminus)	IF	1:200	HPA029674	Sigma-Aldrich
anti-CCDC47 (N-terminus)	WB	1:2,000	A305-100A	Bethyl Laboratories
anti-phospho-eIF2α (S52)	WB	1:250	07-760-I	EMD Millipore
anti-total eIF2α	WB	1:1,000	#5324	Cell Signaling Technology
anti-vinculin	WB	1:2,000	V9131	Sigma-Aldrich
anti-V5	WB	1:2,500	R960-25	Invitrogen/Thermo Fisher Scientific

Abbreviations: IF, immunofluorescence; WB, western blot.

Table S4. Summary of additional candidate variants identified in the four probands.

Proband	Gene	Nucleotide Change	Coding Sequence Change	Amino Acid Change	Inheritance	Parent of Origin	gnomAD All	CADD Phred Score
1	*UBE2V2*	Chr8:g.48962412_48962415 del	NM_003350.2:c.166-1_168del*	Exon 3 skipping (empirical determination)	*de novo*	None	0.000%	32
1	*TAF1A*	Chr1:g.222732051C>T	NM_001201536.1:c.1304G>A	p.(Arg435Glu)	Compound heterozygous	M	0.548%	17.83
		Chr1:g.222737470G>A	NM_001201536.1:c.895-3C>T	NA		P	0.328%	13.81
1	*BCDIN3D-AS1*	Chr12:g.50222535C>G	NR_027500.1:n.202+8C>G	NA	Homozygous	Both	0.633%	12.46
2	*PFKFB2*	Chr1:g.207244919G>T	NM_006212.2:c.1350+1G>T	NA	Homozygous	Both	0.002%	25.4
2	*LUM*	Chr12:g.91498052A>G	NM_002345.3:c.907T>C	p.(Tyr303His)	Homozygous	Both	0.000%	24.9
2	*SEC16A*	Chr9:g.139342104G>A	NM_014866.1:c.6476C>T	p.(Ser2159Leu)	Homozygous	Both	0.004%	23
2	*ACSL4*	ChrX:g.108912383T>C	NM_004458.2:c.1022A>G	p.(Tyr341Cys)	Hemizygous	M	0.000%	21.3
2	*MXRA5*	ChrX:g.3239651C>A	NM_015419.3:c.4075G>T	p.(Val1359Phe)	Hemizygous	M	0.005%	18.45
3	*ZNF780A*	hg38. chr19: 40074802T>G	NM_001142578:c.1640A>C	p.(His547Pro)	*de novo*	NA	0.000%	25.9
3	*GOLGA3*	hg38.chr12: 132807915C>T	NM_001172557:c.1154G>A	p.(Ser385Asn)	Homozygous	Both	0.000%	25.8
3	*ABCA6*	hg38.chr17: 69106070C>T	NM_080284:c.2531G>A	p.(Arg844His)	Homozygous	Both	0.000%	15.26
3	*TUBGCP5*	hg38.chr15 23003072T>C	NM_052903:c.2920A>G	p.(Thr974Ala)	Homozygous	Both	0.000%	NA
3	*GNAI1*	hg38.chr7: 80199301T>C	NM_002069:c.380T>C	p.(Ile127Thr)	Homozygous	Both	0.002%	24.3
4	*ANXA9*	hg38.chr1: 150987933G>C	NM_003568:c.674G>C	p.(Arg225Pro)	*de novo*	NA	0.000%	32
4	*LRRK1*	hg38.chr15:101010676A>G	NM_024652:c.1120A>G	p.(Thr374Ala)	Compound heterozygous	M	0.000%	23
		hg38.chr15: 101065877G>A	NM_024652:c.5440G>A	p.(Ala1814Thr)		P	0.003%	18.55

Abbreviations: CADD, Combined Annotation Dependent Depletion; gnomAD, Genome Aggregation Database; M, maternal; NA, not applicable; P, paternal.

SUPPLEMENTAL METHODS

Enrollment and consent

Proband 1 was evaluated through the National Institutes of Health Undiagnosed Diseases Program and was enrolled in the protocol 76-HG-0238, approved by the National Human Genome Research Institute Institutional Review Board. Her mother provided written informed consent.

Proband 2 was clinically diagnosed at Dr. Sami Ulus Research and Training Hospital of Women's and Children's Health and Diseases and enrolled in the protocol H-29697, approved by Baylor College of Medicine Institutional Review Board. His parents and two siblings provided written informed consent.

Probands 3 and 4 were clinically assessed and followed at The Community Health Clinic (Topeka, IN) and were recruited for research studies through the Clinic for Special Children under a Lancaster General Hospital Institutional Review Board approved protocol. Probands 3 and 4 were also enrolled in the protocol 76-HG-0238, approved by the National Human Genome Research Institute Institutional Review Board for sample collection and molecular analyses. Their parents provided written informed consent.

Isolation and culture of primary cells

Primary dermal fibroblast cells from Probands 1, 3, and 4 were cultured from forearm skin biopsies. Unaffected pediatric sex-matched primary dermal fibroblast cell lines GM01651 (Control 1), GM01652 (Control 2), and GM00038 (Control 3) (Coriell Institute for Medical Research, Camden, NJ) were used as controls. Fibroblasts were cultured in high glucose DMEM (11965092, Gibco/Thermo Fisher Scientific, Gaithersburg, MD) with 10% fetal bovine serum

(FBS, 10082, Gibco/Thermo Fisher Scientific, Gaithersburg, MD) and 1× antibiotic-antimycotic (15240, Gibco/Thermo Fisher Scientific, Gaithersburg, MD) (complete DMEM) at 37°C with 5% CO_2.

Lymphoblastoid cell lines were established from the peripheral blood samples of Proband 2 and his father and unaffected sibling by transformation with Epstein-Barr virus (EBV)-containing supernatant as previously described.[1]

Lymphoblastoid cells were cultured in RPMI 1640 Medium with GlutaMAX Supplement (61870036, Gibco/Thermo Fisher Scientific, Gaithersburg, MD) containing 10% FBS (10082, Gibco/Thermo Fisher Scientific, Gaithersburg, MD) and 1× antibiotic-antimycotic (15240, Gibco/Thermo Fisher Scientific, Gaithersburg, MD) (complete RPMI) at 37°C with 5% CO_2.

Whole exome sequencing analysis

Whole exome sequencing analysis was performed on the probands and their parents at 3 centers: Proband 1 at the National Institutes of Health Intramural Sequencing Center (NISC), Proband 2 through the Baylor-Hopkins Center for Mendelian Genomics (BHCMG), and Probands 3 and 4 at the Regeneron Genetics Center through the collaboration with the Clinic for Special Children.

With respect to the identification of potential collaborators who had identified *CCDC47* as a candidate gene and from the perspective of the National Institutes of Health, we initially submitted *CCDC47* to GeneMatcher, an online tool for connecting researchers with an interest in the same gene;[2] no additional cases with a similar constellation of phenotypic features and rare variation in *CCDC47* were identified. We next contacted Jill A. Mokry at the Baylor College of Medicine to look through the Baylor-Hopkins Center for Mendelian Genetics (BHCMG) database, which facilitated the collaboration with the Lupski Lab and identification of Proband 2.

Finally, identification of Probands 3 and 4 were the result of a serendipitous conversation while Dr. Kevin A. Strauss from the Clinic for Special Children was visiting the Undiagnosed Diseases Program.

Peripheral whole blood samples were collected from Proband 1 and her parents. DNA was extracted using the AutoGen FLEX STAR automated genomic DNA extraction and isolation system. The DNA samples were purified by phenol-chloroform extraction and sent to the NISC for whole exome sequence analysis. Sequencing libraries with approximately 300 bp inserts and paired-end index adapters were prepared and enriched for targeted whole exome regions using the TruSeq DNA Sample Prep Kit v1 (Illumina, San Diego, CA) and sequenced on the HiSeq 2000 Sequencing System (Illumina, San Diego, CA) for 101-bp paired-end reads. The sequencing reads then were filtered for quality and aligned to human reference genome NCBI build 37 (hg19) using pipeline developed by the Undiagnosed Diseases Program (UDP), one based on NovoAlign (Novocraft Technologies, Petaling Jaya, Malaysia), and separately, a diploid aligner[3] that was run on a commercial platform (Appistry Inc., St. Louis, MO). Variants were called with HaplotypeCaller and GenotypeGVCFs.[4-6] Variants were annotated using snpEff[7] and a combination of publicly available data sources (ExAC, ESP, 1000Genomes, see URLs) and internal cohort statistics. These annotations were utilized in the variant analysis method developed at the UDP in which rare, non-synonymous, start-gain/loss, stop-gain/loss, frameshift, canonical splice site variants and intronic variants (± 20 bp) that were consistent with homozygous recessive, compound heterozygous, X-linked or *de novo* dominant disease models were retained. These variants were manually inspected using the Integrative Genomics Viewer (IGV) and checked for publicly available clinical or functional data in OMIM, HGMD, and PubMed. Variants were interpreted and prioritized based on the clinical relevance of the gene

and the pathogenicity of the variants using the ACMG-AMP guidelines.[8] In the absence of candidate variants with unambiguous clinical relevance such as those in the majority of UDP cases and in this case in particular, variants were prioritized by inferred significance based on Mendelian consistency, population frequency, and predicted deleteriousness, coalesced with published biological and functional data of the genes.

Whole exome sequencing was performed on Proband 2 and his sibling (2: II-1) at Baylor College of Medicine Human Genome Sequencing Centre (BCM-HGSC) through the Baylor-Hopkins Center for Mendelian Genomics (BHCMG) initiative using previously described procedure.[9] In brief, peripheral blood samples were collected from Proband 2, his parents and two unaffected siblings. Genomic DNA was extracted from the blood samples using the Gentra PureGene Blood Kit (Qiagen Sciences Inc., Germantown, MD). The sequencing libraries were constructed using the SeqCap EZ HGSC VCRome Kit (Roche NimbleGen) with the VCRome 2.1 exome capture design and sequenced on the HiSeq 2500 Sequencing System (Illumina, San Diego, CA) with ~100× depth of coverage. Sequencing data processing and variant annotation were performed using the Mercury pipeline.[10] Variants were evaluated based on a homozygous recessive, compound heterozygous or *de novo* dominant disease model with a minor allelic frequency (MAF) less than 0.001, 0.0005 and 0.0001 accordingly within the BHCMG in-house database, NHLBI Exome Sequencing Project Exome Variant Server (ESP 5400), 1000 Genomes, and the Exome Aggregation Consortium (ExAC) Browser.

We performed family whole exome sequencing for Probands 3 and 4, their unaffected parents and all available unaffected siblings. Genomic DNA was extracted from peripheral blood samples and submitted for whole exome sequencing in collaboration with the Regeneron Genetics Center (RGC). Fluorescence-based quantification was performed to ensure appropriate

DNA quantity and quality for sequencing purposes. One μg of DNA was sheared to an average fragment length of 150 base pairs (Covaris LE220) and prepared for exome capture with a custom reagent kit from Kapa Biosystems. Samples were captured using the IDT xGen exome capture reagent (Integrated DNA Technologies, Coralville, IA). Samples were barcoded, pooled, and multiplexed using 75 bp paired-end sequencing on an Illumina HiSeq 2500 with v4 chemistry (Illumina, San Diego, CA). Captured fragments were sequenced to achieve a minimum of 85% of the target bases covered at 20× or greater coverage. Following sequencing, data was processed using a cloud-based pipeline developed at the RGC that uses DNAnexus and AWS to run standard tools for sample-level data production and analysis. Sequence reads were mapped and aligned to the GRCh38/hg38 human genome reference assembly using BWA-mem. After alignment, duplicate reads were marked and flagged. SNP and INDEL variants and genotypes were called using GATK's HaplotypeCaller. Called variants were further analyzed using an RGC implemented bioinformatics pipeline for family-based analyses as previously reported.[11] Briefly, standard quality-control filters (read depth ≥10, genotype quality ≥30, allelic balance ≥20%) were applied to called variants. Passing variants were classified and annotated based on their potential functional effects using RefSeq and ENSEMBL75 transcripts. We verified familial relationships through identity-by-descent (IBD) derived metrics from genetic data to infer relatedness and relationships in our cohort using PRIMUS[12] and cross-referencing with reported pedigrees. Variants were subsequently annotated and filtered by their observed frequencies in population control databases such as dbSNP, the 1000 Genomes Project, the NHLBI Exome Sequencing Project, the Exome Aggregation Consortium Database (ExAC), and internal RGC databases in order to filter out common polymorphisms and high frequency, likely benign variants. Algorithms for bioinformatic prediction of functional effects of variants, such as

LRT, PolyPhen-2, SIFT, CADD, and MutationTaster; along with conservation scores based on multiple species alignments (i.e. GERP, PhastCons, PhyloP) were incorporated as part of the annotation process of variants and used to inform on the potential deleteriousness of identified candidate variants.

Segregation with disease status in all available family members was subsequently verified for all candidate variants identified in each pedigree. Analyses were guided according to the pedigree information and the genetically verified familial relationships and structure. For Proband 3, we identified 6 candidate variants in 6 genes (5 homozygous and 1 *de novo*), however all other recessive variants had 1-8 homozygous individuals reported in population databases except for a homozygous rare frameshift mutation [hg38.chr17:63752378(delA); c.1145delT; p.(Leu382Argfs*2)] in *CCDC47*. For Proband 4, analyses identified 4 candidate variants in 3 genes (1 homozygous, 1 compound heterozygous and 1 *de novo*). One of the compound heterozygous variants was observed in homozygosis in 10 individuals in population databases and subsequently deprioritized. The proband also was homozygous for the p.(Leu382Argfs*2) frameshift variant. Given the predicted effect of the mutation likely leading to loss-of-function of the candidate gene and the striking phenotypic similarity between the two probands, we identified *CCDC47* as the main candidate for the phenotype in these individuals.

All candidate variants identified through whole exome sequencing analysis were validated by Sanger sequencing.

RNA extraction and reverse transcription

Cells were homogenized using the QIAshredder (79654, Qiagen, Germantown, MD) and total RNA was extracted using the RNeasy Mini Kit (74106, Qiagen, Germantown, MD). Genomic DNA was removed by on-column DNase I digestion (79254, Qiagen, Germantown, MD).

Reverse transcription was performed using the Omniscript Reverse Transcription Kit (205111, Qiagen, Germantown, MD) using 1.5 μg total RNA per reaction according to the manufacturer's specifications.

Gene expression analysis

TaqMan Gene Expression Master Mix (4369016, Applied Biosystems/Thermo Fisher Scientific, Foster City, CA) was used with the 7500 Fast Real-Time PCR System (Applied Biosystems/Thermo Fisher Scientific, Foster City, CA) for gene expression analysis. The following conditions were used for amplification: 1 cycle of 50°C for 2 min for uracil-N-glycosylase incubation, followed by 1 cycle of 95°C for 10 min for DNA polymerase activation, followed by 40 cycles of 95°C for 15 s and 60°C for 1 min for PCR amplification.

The relative quantification of gene expression was calculated using the delta-delta C_t method[13] using the 7500 Software version 2.3 (Applied Biosystems/Thermo Fisher Scientific, Foster City, CA). Expression of at least two of the following genes were used as the internal control: *HPRT1*, *POLR2A*, and/or *TBP*. All TaqMan assays used for gene expression analysis are presented in Table S1.

***XBP1* splicing assay**

Cells were treated with the sarco/endoplasmic reticulum Ca^{2+} ATPase (SERCA) inhibitor thapsigargin at a concentration of 100 nM to induce endoplasmic reticulum stress for 0, 0.5, 1, 2,

4, or 8 hours. Total RNA was extracted as described above and reverse transcription was performed as described above with 0.5 μg of total RNA per reaction.

Upon ER stress, the unfolded protein response (UPR) is activated and IRE1-alpha phosphorylation leads to splicing of the X-box binding protein 1 (*XBP1*) mRNA.[14] Primers specific to spliced *XBP1* mRNA[15] were used for quantitative PCR (Table S2). 2× QuantiFast SYBR Green PCR Master Mix (204056, Qiagen, Germantown, MD) was used with the 7500 Fast Real-Time PCR System (Applied Biosystems/Thermo Fisher Scientific, Foster City, CA) for *XBP1* splicing analysis. The following conditions were used for amplification: 1 cycle of 95°C for 5 min for DNA polymerase activation, followed by 40 cycles of 95°C for 10 s and 60°C for 30 s, followed by a melt curve analysis.

The relative quantification of gene expression was calculated as above, using *TBP1* as an internal control. All primers used for the *XBP1* splicing assay are presented in Table S2.

Western blot analysis

Cells were lysed in RIPA Buffer (R0278, Sigma-Aldrich, St. Louis, MO) containing 1× Complete Protease Inhibitor Cocktail (05892970001, Roche/Sigma-Aldrich, St. Louis, MO) and 1× PhosSTOP phosphatase inhibitor (04906837001, Roche/Sigma-Aldrich, St. Louis, MO) for 15 min on ice. The samples were homogenized (Model 250 Digital Sonifier, Branson Ultrasonics, Danbury, CT) at 10% amplitude for 30 s on ice. Laemmli sample buffer was added and samples were boiled for 5 min and resolved on a 4-15% gradient polyacrylamide gel and transferred to a PVDF membrane. Membranes were blocked using Odyssey Blocking Buffer (LI-COR Biosciences, Lincoln, NE) for 1 hour at room temperature and subsequently incubated with primary antibodies diluted in Odyssey Blocking Buffer with 0.1% Tween 20 overnight at 4°C.

After four 5-min washes with PBS-T (0.1% Tween 20 in phosphate buffered saline or PBS) or TBS-T (0.1% Tween 20 in Teen-buffered saline or TBS), membranes were incubated with IRDye-conjugated secondary antibodies (LI-COR Biosciences, Lincoln, NE) for 1 hour at room temperature. After four 5-min washes with PBS-T or TBS-T, two 5-min washes with PBS or TBS were performed to remove residual Tween 20. Membranes were imaged on the Odyssey CLx Infrared Imaging System and analyzed using the CLx Image Studio version 3.1 software (LI-COR Biosciences, Lincoln, NE). All primary antibodies and dilutions used for western blot are presented in Table S3.

Indirect immunofluorescence

Unaffected control and Proband 1 fibroblasts were plated at 5×10^4 cells per well on coverslips in a 6-well plate and cultured overnight. All staining procedures were performed at room temperature unless specified otherwise. Cells were washed with PBS, then fixed with 4% paraformaldehyde (Electron Microscopy Sciences, Hatfield, PA) for 15 min, washed three times with PBS, permeabilized with 0.5% Triton X-100 in PBS for 10 min, and washed once with PBS. Endogenous peroxidases were quenched with 0.3% hydrogen peroxide in PBS for 20 min. Cells were washed with PBS, incubated with blocking buffer (5% normal goat serum, 1% bovine serum albumin in PBS) for 1 hour, and subsequently incubated with primary antibodies against CCDC47 (1:200, HPA029674, Sigma-Aldrich) and the ER marker calnexin (1:100, MAB3126, EMD Millipore) diluted in blocking buffer overnight at 4°C. After four 10-min washes with PBS, cells were incubated with Alexa Fluor-conjugated secondary antibody (1:1,000, Invitrogen/Thermo Fisher Scientific, Carlsbad, CA) to detect anti-calnexin or HRP-conjugated secondary antibody with the Tyramide Signal Amplification Kit (Invitrogen/Thermo Fisher

Scientific, Carlsbad, CA) according to the manufacturer's specifications to detect anti-CCDC47. Following four 10-min washes with 1× PBS, cells were mounted with ProLong Gold Antifade Mountant with DAPI (Invitrogen/Thermo Fisher Scientific, Carlsbad, CA) and cured for 24 hours.

Images were acquired using a 63×/1.4 oil DIC Plan-APOCHROMAT objective lens on an LSM 700 laser scanning confocal microscope (Carl Zeiss Microscopy, Jena, Germany) with the ZEN 2012 SP1 (black edition) version 8.1 software (Carl Zeiss Microscopy, Jena, Germany).

Ca^{2+} imaging

Elevation of cytoplasmic Ca^{2+} following the addition of 2 μM thapsigargin to assess total ER Ca^{2+} levels, 0.5 μM IP_3-AM to assess Ca^{2+} release from the ER via the inositol 1,4,5-triphosphate receptor (IP_3R), 10 μM ryanodine to assess Ca^{2+} release from the ER via the ryanodine receptor (RyR), and 0.2 μM thapsigargin to assess Ca^{2+} leak from the ER via ion channels, including presenilin 1 and bax inhibitor 1,[16,17] to unaffected control fibroblasts, Proband 1, 3, 4 fibroblasts, and Proband 1 fibroblasts overexpressing wild type *CCDC47* was measured using the cell permeable Ca^{2+} indicator Fura-2, AM (Invitrogen/Thermo Fisher Scientific, Carlsbad, CA) with an excitation at 340 and 380 nm and emission at 525 nm. Ionomycin, a selective Ca^{2+} ionophore that raises intracellular Ca^{2+} levels,[18,19] was added to check cell viability. Store-operated Ca^{2+} entry (SOCE) was assessed by pretreatment of the cells with 2 μM thapsigargin to induce emptying of the ER Ca^{2+} store, followed by addition of 2 mM $CaCl_2$ to trigger ER store refilling. Ca^{2+} release was calculated ratiometrically between emissions of 340 and 380 nm. Cells in Ibidi chamber slides (Thistle Scientific, UK) were washed once in cold medium with 1% bovine serum albumin (BSA). Subsequently, cells were incubated at 16°C

for 1 hour with 5 μM Fura-2, AM in complete DMEM (10% fetal calf serum, 1× L-glutamine) with 1% BSA and 0.025% Pluronic F-127 (Sigma). The Fura-2, AM solution was then removed, and the cells were incubated in complete HBSS (supplemented with 5 mM HEPES (pH 7.2), 1 mM $MgCl_2$ and no $CaCl_2$) for 10 min to allow esterases within the cells to cleave the acetoxymethyl ester group on the probe, which would otherwise inhibit fluorescence. Cells were then washed twice with complete HBSS and imaged live using a Zeiss Axiovert 35 with an ORCA Flash 4.0 lite sCMOS camera, Cairn Optospin filter wheels, xCite 120 HXP fluorescence lamp and Metafluor software. Ca^{2+} traces and statistical analyses were then performed using GraphPad Prism 6.0. Data were analyzed using one-way ANOVA with Fischer post-hoc tests.

Oxidative stress assay

Fibroblasts were plated at 2.5×10^3 cells per well in a 96-well plate. To determine their susceptibility to oxidative stress, the cells were treated with the glutathione synthesis inhibitor L-buthionine-(*S*,*R*)-sulfoximine (BSO) at a concentration of 25 or 50 μM and increasing concentrations of iron (Fe^{3+} citrate) for 48 hours to increase their oxidative burden. The cell viability was measured with Calcein-AM.

Utilizing the oxidative stress condition where unaffected control cells were least affected while the Proband 1 cells exhibited <10% viability, the compound EPI-743 (Edison Pharmaceuticals Inc./BioElectron Technology, Mountain View, CA), which has shown efficacy in rescuing cells from individuals with primary genetic mitochondrial disease,[20,21] was tested between the concentrations of 1-1000 nM. The EC_{50} was calculated via and Prism (GraphPad Software, La Jolla, CA) utilizing the 4-parameter sigmoidal dose-response (variable slope) model.

CCDC47 cloning and lentiviral transduction

A *CCDC47* TrueORF Clone (RC203425, Origene Technologies, Rockville, MD) was used to amplify a *CCDC47* ORF with and without a stop codon by PCR with the Platinum *Pfx* DNA Polymerase using the following conditions for amplification: 1 cycle of 94°C for 5 minutes for template denaturation; followed by 40 cycles of 94°C for 15 seconds, 60°C for 30 seconds, and 68°C for 90 seconds; followed by a final extension at 68°C for 10 minutes. Primer sequences used for amplifying the *CCDC47* ORF are presented in Table S2.

PCR products were then cloned into the pENTR entry vector using the pENTR/D-TOPO Cloning Kit (Invitrogen/Thermo Fisher Scientific, Carlsbad, CA). Single clones were Sanger sequenced to verify the insertion and sequence integrity of the *CCDC47* ORF and a Maxiprep was performed using the Plasmid Plus Maxi Kit (Qiagen, Germantown, MD). LR recombination was performed using the Gateway LR Clonase II Enzyme Mix (Invitrogen/Thermo Fisher Scientific, Carlsbad, CA) to recombine the *CCDC47* ORF into the pLenti6.3 destination vector. Singles clones were Sanger sequenced to verify the recombination and sequence integrity of the *CCDC47* ORF and a Maxiprep was performed using the Plasmid Plus Maxi Kit (Qiagen, Germantown, MD). Primer sequences used for sequencing the *CCDC47* ORF in the pENTR and pLenti6.3 vectors are presented in Table S2.

The ViraPower Lentiviral Expression System (Invitrogen/Thermo Fisher Scientific, Carlsbad, CA) was used to overexpress *CCDC47* in the patient cell line. In brief, lentivirus was generated by transfecting 293FT cells with the pLenti6.3-*CCDC47* construct and the ViraPower Packaging Mix using Lipofectamine 2000 (Invitrogen/Thermo Fisher Scientific, Carlsbad, CA). The fibroblasts from Proband 1 were transduced with the viral supernatant and stable cell lines

were selected for by the addition of 1 μg/ml blasticidin to the complete DMEM. Overexpression of *CCDC47* mRNA and CCDC47 protein were confirmed by TaqMan gene expression assay and western blot. TaqMan gene expression assays and antibodies used for western blot are presented in Tables S1 and S3.

Absence of heterozygosity (AOH) analysis

Absence of heterozygosity (AOH) was bioinformatically determined by calculating a B-allele frequency from exome data using BafCalculator (https://github.com/BCM-Lupskilab/BafCalculator). B-allele frequency was calculated by the ratio of variant to total reads at each base position. The Circular Binary Segmentation algorithm of the DNAcopy package in R was utilized to determine genomic segments within which the DNA copy status is consistent. After subtracting 0.5 from the calculated B-allele frequency, the genomic intervals with a mean signal >0.45 and have a length >1 kb were predicted to be regions of AOH that potentially demonstrate identity-by-descent (IBD).[22,23]

SUPPLEMENTAL REFERENCES

1. Tosato, G., and Cohen, J.I. (2007). Generation of Epstein-Barr Virus (EBV)-immortalized B cell lines. Curr. Protoc. Immunol. *Chapter 7*, Unit 7.22.
2. Sobreira, N., Schiettecatte, F., Valle, D., and Hamosh, A. (2015). GeneMatcher: A matching tool for connecting investigators with an interest in the same gene. Hum. Mutat. *36*, 928-930.
3. Pemberton, P.J., Valkanas, E., Bone, W.P., Markello, C.J., Flynn, E.D., Links, A.E., Boerkoel, C.F., Adams, D.R., Gahl, W.A., Markello, T.C., NIH Intramural Sequencing Center, NIH Genomics Core, UDP Clinical Team. (2014). Diploid alignment of whole human genome data. In 64th Annual Meeting of the American Society of Human Genetics. (San Diego, CA).
4. McKenna, A., Hanna, M., Banks, E., Sivachenko, A., Cibulskis, K., Kernytsky, A., Garimella, K., Altshuler, D., Gabriel, S., Daly, M., et al. (2010). The Genome Analysis Toolkit: A MapReduce framework for analyzing next-generation DNA sequencing data. Genome Res. *20*, 1297-1303.
5. DePristo, M.A., Banks, E., Poplin, R., Garimella, K.V., Maguire, J.R., Hartl, C., Philippakis, A.A., del Angel, G., Rivas, M.A., Hanna, M., et al. (2011). A framework for variation discovery and genotyping using next-generation DNA sequencing data. Nat. Genet. *43*, 491-498.
6. Van der Auwera, G.A., Carneiro, M.O., Hartl, C., Poplin, R., Del Angel, G., Levy-Moonshine, A., Jordan, T., Shakir, K., Roazen, D., Thibault, J., et al. (2013). From FastQ data to high confidence variant calls: The Genome Analysis Toolkit best practices pipeline. Curr. Protoc. Bioinformatics *43*, 11.10.11-33.
7. Cingolani, P., Platts, A., Wang le, L., Coon, M., Nguyen, T., Wang, L., Land, S.J., Lu, X., and Ruden, D.M. (2012). A program for annotating and predicting the effects of single nucleotide polymorphisms, SnpEff: SNPs in the genome of Drosophila melanogaster strain w1118; iso-2; iso-3. Fly *6*, 80-92.
8. Richards, S., Aziz, N., Bale, S., Bick, D., Das, S., Gastier-Foster, J., Grody, W.W., Hegde, M., Lyon, E., Spector, E., et al. (2015). Standards and guidelines for the interpretation of sequence variants: A joint consensus recommendation of the American College of Medical Genetics and Genomics and the Association for Molecular Pathology. Genet. Med. *17*, 405-424.
9. Lupski, J.R., Gonzaga-Jauregui, C., Yang, Y., Bainbridge, M.N., Jhangiani, S., Buhay, C.J., Kovar, C.L., Wang, M., Hawes, A.C., Reid, J.G., et al. (2013). Exome sequencing resolves apparent incidental findings and reveals further complexity of *SH3TC2* variant alleles causing Charcot-Marie-Tooth neuropathy. Genome Med. *5*, 57.
10. Reid, J.G., Carroll, A., Veeraraghavan, N., Dahdouli, M., Sundquist, A., English, A., Bainbridge, M., White, S., Salerno, W., Buhay, C., et al. (2014). Launching genomics into the cloud: Deployment of Mercury, a next generation sequence analysis pipeline. BMC Bioinformatics *15*, 30.
11. Strauss, K.A., Gonzaga-Jauregui, C., Brigatti, K.W., Williams, K.B., King, A.K., Van Hout, C., Robinson, D.L., Young, M., Praveen, K., Heaps, A.D., et al. (2018). Genomic diagnostics within a medically underserved population: Efficacy and implications. Genet. Med. *20*, 31-41.

12. Staples, J., Qiao, D., Cho, M.H., Silverman, E.K., Nickerson, D.A., and Below, J.E. (2014). PRIMUS: Rapid reconstruction of pedigrees from genome-wide estimates of identity by descent. Am. J. Hum. Genet. *95*, 553-564.
13. Livak, K.J., and Schmittgen, T.D. (2001). Analysis of relative gene expression data using real-time quantitative PCR and the $2^{-\Delta\Delta CT}$ Method. Methods *25*, 402-408.
14. Yoshida, H., Matsui, T., Yamamoto, A., Okada, T., and Mori, K. (2001). *XBP1* mRNA is induced by ATF6 and spliced by IRE1 in response to ER stress to produce a highly active transcription factor. Cell *107*, 881-891.
15. van Schadewijk, A., van't Wout, E.F., Stolk, J., and Hiemstra, P.S. (2012). A quantitative method for detection of spliced X-box binding protein-1 (*XBP1*) mRNA as a measure of endoplasmic reticulum (ER) stress. Cell Stress Chaperones *17*, 275-279.
16. Nelson, O., Tu, H., Lei, T., Bentahir, M., de Strooper, B., and Bezprozvanny, I. (2007). Familial Alzheimer disease-linked mutations specifically disrupt Ca^{2+} leak function of presenilin 1. J. Clin. Invest. *117*, 1230-1239.
17. Bultynck, G., Kiviluoto, S., and Methner, A. (2014). Bax inhibitor-1 is likely a pH-sensitive calcium leak channel, not a H^+/Ca^{2+} exchanger. Sci. Signal *7*, pe22.
18. Yoshida, S., and Plant, S. (1992). Mechanism of release of Ca^{2+} from intracellular stores in response to ionomycin in oocytes of the frog *Xenopus laevis*. J. Physiol. *458*, 307-318.
19. Morgan, A.J., and Jacob, R. (1994). Ionomycin enhances Ca^{2+} influx by stimulating store-regulated cation entry and not by a direct action at the plasma membrane. Biochem. J. *300 (Pt 3)*, 665-672.
20. Shrader, W.D., Amagata, A., Barnes, A., Enns, G.M., Hinman, A., Jankowski, O., Kheifets, V., Komatsuzaki, R., Lee, E., Mollard, P., et al. (2011). alpha-Tocotrienol quinone modulates oxidative stress response and the biochemistry of aging. Bioorg. Med. Chem. Lett. *21*, 3693-3698.
21. Enns, G.M.C., B. H. (2017). Clinical trials in mitochondrial disease: An update on EPI-743 and RP103. J. Inborn Errors Metab. Screen. *5*, 1-7.
22. Gambin, T., Akdemir, Z.C., Yuan, B., Gu, S., Chiang, T., Carvalho, C.M.B., Shaw, C., Jhangiani, S., Boone, P.M., Eldomery, M.K., et al. (2017). Homozygous and hemizygous CNV detection from exome sequencing data in a Mendelian disease cohort. Nucleic Acids Res. *45*, 1633-1648.
23. Karaca, E., Posey, J.E., Coban Akdemir, Z., Pehlivan, D., Harel, T., Jhangiani, S.N., Bayram, Y., Song, X., Bahrambeigi, V., Yuregir, O.O., et al. (2018). Phenotypic expansion illuminates multilocus pathogenic variation. Genet. Med. https://doi.org/10.1038/gim.2018.33